Dalton Transactions

An international journal of inorganic chemistry

www.rsc.org/dalton

Volume 42 | Number 31 | 21 August 2013 | Pages 11023–11328

ISSN 1477-9226

RSC Publishing

COVER ARTICLE
Piguet *et al*.
Monitoring helical twists and effective molarities in dinuclear triple-stranded lanthanide helicates

1477-9226(2013)42:31;1-M

Dalton Transactions

RSC Publishing

PAPER

Monitoring helical twists and effective molarities in dinuclear triple-stranded lanthanide helicates†

Cite this: *Dalton Trans.*, 2013, **42**, 11047

Patrick E. Ryan,[a] Laure Guénée[b] and Claude Piguet*[a]

Received 9th April 2013,
Accepted 29th April 2013

DOI: 10.1039/c3dt50941a

www.rsc.org/dalton

The replacement of terminal benzimidazole–pyridine binding units in the neutral di-tridentate segmental ligand **L1** with phenanthroline in **L10** reduces the number of torsional degrees of freedom by two units. Reactions of these ligands with trivalent europium or lutetium cations yield structurally similar self-assembled dinuclear triple-stranded $[Ln_2(\mathbf{L}\boldsymbol{k})_3]^{6+}$ complexes, thus demonstrating that the increased rigidity of the strand in **L10** is compatible with its helical twist. With the larger lanthanum cations, the metallic coordination spheres are completed with two terminal axial triflate counter-anions to give $[La_2(\mathbf{L10})_3(CF_3SO_3)_2]^{4+}$. Thermodynamic investigations in acetonitrile confirm the minor constraints produced by the planar phenanthroline unit in **L10** leading to comparable effective molarities $EM^{Eu,\mathbf{L1}} \approx EM^{Eu,\mathbf{L10}} = 10^{-3.9(4)}$ M with mid-range Eu^{III} cations. The striking minute effective molarities $EM^{Ln,\mathbf{Ln}\text{-}2H} \approx 10^{-6}$–$10^{-9}$ M obtained upon the replacement of terminal phenanthrolines with structurally analogous fused hydroxyquinolines in **L9** can be thus unambiguously assigned to solvation effects, a new tool for controlling complexity in metal-induced self-assembly processes.

Introduction

The extension of the principle of maximum occupancy,[1] originally set for the design of polynuclear helicates with 4-coordinated and 6-coordinated d-block cations in metallosupramolecular chemistry,[2] led to the isolation of the first triple-stranded dinuclear lanthanide helicates by reacting nine-coordinated 4f-block cations with the di-tridentate ligand **L1**.[3] Since then, the helical twist induced by diphenylmethane spacers was systematically exploited in homotopic (**L2**,[4] **L3**[5] and **L4**[6]) and heterotopic (**L5**[7] and **L6**[8]) segmental di-tridentate ligands for producing lanthanide helicates working as luminescent bioprobes[9] with unprecedented thermodynamic selectivities.[3d,7] Structural analyses suggested that the successive non-negligible inter-aromatic torsions observed along the ligand strands were a pre-requisite for a successful helication (see Scheme 1), and related segmental ligands with an increasing number of torsional degrees of freedom such as **L7**[10] (and derivatives of it)[11] or **L8**[12] indeed provided stable triple-stranded lanthanide helicates.

Whereas kinetic studies rapidly delivered pertinent models for the time evolution of the assembly processes leading to dinuclear lanthanide helicates,[13] the rationalization of the thermodynamic driving forces responsible for the apparent selective formation of a single species was delayed until Ercolani used the concept of effective molarity (EM) for satisfyingly modelling the intramolecular metal–ligand binding events responsible for the formation of metallosupramolecular edifices (eqn (1) and Fig. 1).[14]

$$EM = \frac{K_{intra}}{K_{inter}} = e^{\left(\frac{\Delta G_{inter}-\Delta G_{intra}}{RT}\right)} \quad (1)$$

Taking the well-accepted concentration of $c^\theta = 1$ M for the reference state,[15] the van't Hoff isotherm transforms EM into the free energy contribution $\Delta G_{intra} - \Delta G_{inter} = -RT\ln(EM/c^\theta)$, which estimates the advantage (EM > 1 M) or drawback (EM < 1 M) produced by the replacement of an intermolecular connection by its intramolecular counterpart.[16]

The average effective molarity, which controls the intramolecular macrocyclization processes along the assembly of the dinuclear lanthanide triple-stranded helicates $[Eu_2(\mathbf{L}\boldsymbol{k})_3]^{6+}$ (**L*k*** = **L1**–**L2**), amounts to $EM = 10^{-4.1}$ M in acetonitrile.[17] Consequently, any intramolecular binding event is penalized by $\Delta G_{intra} - \Delta G_{inter} = 23.4$ kJ mol^{-1} (eqn (1)), a trend drastically amplified upon reduction of the total number of torsional degrees of freedom along the strands as found in $[Eu_2(\mathbf{L9}\text{-}2H)_3]$ ($EM = 10^{-5.8}$ M, $\Delta G_{intra} - \Delta G_{inter} = 33.1$ kJ mol^{-1}) and in $[Lu_2(\mathbf{L9}\text{-}2H)_3]$ ($EM = 10^{-9}$ M, $\Delta G_{intra} - \Delta G_{inter} = 51.3$ kJ mol^{-1}).[18] Given that $\Delta G_{inter}^{Eu,\mathbf{L1}} = -30$ kJ mol^{-1} (ref. 17) and $\Delta G_{inter}^{Ln,\mathbf{L9}\text{-}2H} \approx$

[a]Department of Inorganic and Analytical Chemistry, University of Geneva, 30 quai E. Ansermet, CH-1211 Geneva 4, Switzerland. E-mail: Claude.Piguet@unige.ch
[b]Laboratory of X-ray Crystallography, University of Geneva, 24 quai E. Ansermet, CH-1211 Geneva 4, Switzerland

†Electronic supplementary information (ESI) available. CCDC 933010 and 933011. For ESI and crystallographic data in CIF or other electronic format see DOI: 10.1039/c3dt50941a

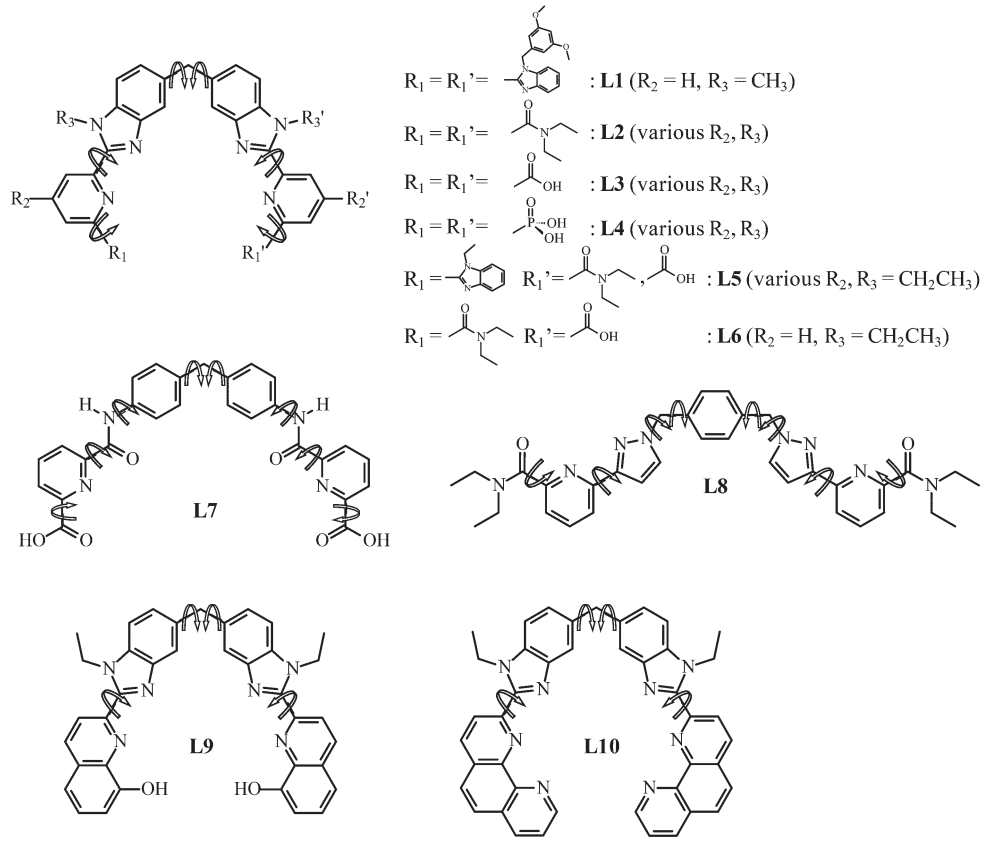

Scheme 1 Chemical structures of the segmental di-tridentate ligands **L1–L10**. The curved arrows highlight the torsional degrees of freedom.

−40 kJ mol^{-1} (ref. 18), the energetic contribution induced by the effective molarity represents a crucial parameter for tuning the driving force controlling the overall stability of the final helicates. However, the pertinence of any comparison between ligands **L1** or **L2** (six torsional degrees of freedom, Scheme 1) and **L9** (four torsional degrees of freedom, Scheme 1) is limited by (i) the use of different tridendate donor groups (neutral N_3 or N_2O in **L1** and **L2** and negatively charged N_2O^- in **L9**) and (ii) the consideration of different solvents for imperative solubility reasons (acetonitrile for **L1** and **L2** and dichloromethane–methanol (1 : 1) for **L9**). In order to decipher the real impact of the total number of torsional degrees of freedom on the effective molarity, we report here on the structural and thermodynamic behaviour of the triple-stranded helicates $[Ln_2(\mathbf{L10})_3]^{6+}$, in which the di-tridentate ligand **L10** is expected to be as rigid as $[\mathbf{L9}\text{-}2H]^{2-}$, but as neutral and soluble in acetonitrile as **L1**.

Results and discussion

Synthesis and characterization of ligand and complexes

The di-tridentate ligand **L10** was obtained in five steps from commercially available 1,10-phenanthroline (global yield = 12%, Scheme 2). After oxidation into its *N*-oxide form **1**, a cyano group was introduced *via* a nucleophilic aryl substitution. Reduction yielded **2** whose hydrolysis eventually gave 1,10-phenanthroline-2-carboxylic acid **3**.[19] Activation of the carboxylic group into its acyl chloride followed by coupling with 3,3′-dinitro-4,4′di(*N*-ethyl)amino-diphenylmethane[20] resulted in the di-orthonitroamido compound **4**, which was finally converted into **L10** by reductive cyclization.[21] The nine aromatic signals detected by ^{1}H NMR combined with the existence of three enantiotopic methylene groups were diagnostic of **L10** adopting a dynamically average C_{2v} symmetry in solution (Fig. 2a).[22] The lack of Nuclear Overhauser Enhancement effect between H5 and H7 indicated that the transoid conformation depicted in Scheme 2 was adopted by the benzimidazole–phenanthroline units.

Reaction of **L10** (3 equiv.) with $Ln(CF_3O_3)_3{\cdot}xH_2O$ (Ln = La, Eu, Lu; x = 1–3) in acetonitrile–chloroform (2 : 3) gave 62–93% of the dinuclear complexes $[Ln_2(\mathbf{L10})_3](CF_3SO_3)_6{\cdot}xH_2O{\cdot}yCHCl_3$ (Ln = La, x = 3, y = 3; Ln = Eu, x = 7, y = 0; Ln = Lu, x = 5, y = 0). Slow diffusion of benzene or ^{t}butyl-methylether into concentrated acetonitrile solutions of these complexes yielded pale yellow X-ray quality prisms for $[La_2(\mathbf{L10})_3(CF_3SO_3)_2](CF_3SO_3)_4$-$(CH_3CN)_6(C_6H_6)_6$ (**5**) and $[Lu_2(\mathbf{L10})_3](CF_3SO_3)_6(CH_3CN)_4$ (**6**). Both crystal structures contained dinuclear triple helical cations, non-coordinated counter-anions and interstitial solvent molecules (Fig. 3 and S1; Tables S1–S5†).

The molecular structures of $[Lu_2(\mathbf{L10})_3]^{6+}$ and $[Eu_2(\mathbf{L1})_3]^{6+}$ are almost superimposable and globally display one helical

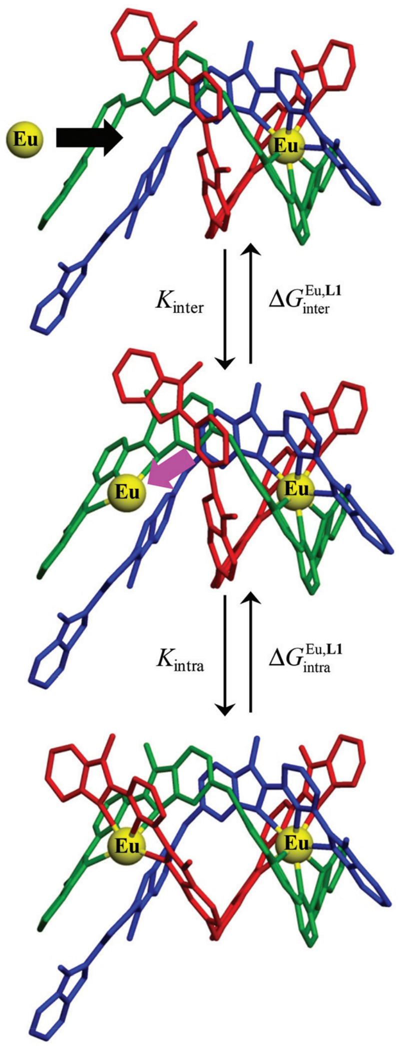

Fig. 1 Illustration of intermolecular (black arrow, top) and intramolecular (pink arrow, bottom) metal–ligand binding processes operating during the self-assembly of $[Eu_2(\mathbf{L1})_3]^{6+}$. Peripheral ligand substituents are omitted for clarity.

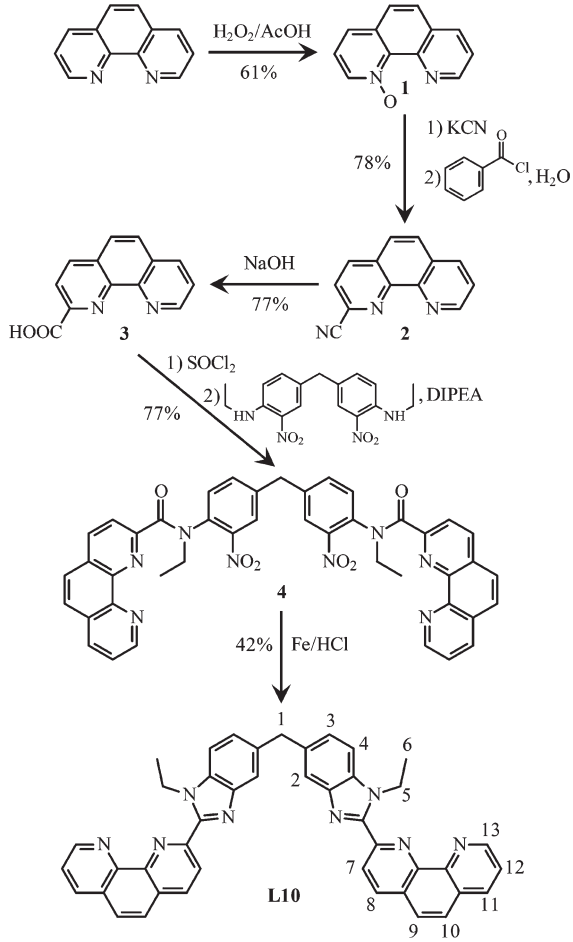

Scheme 2 Synthesis of the ligand **L10** with the numbering scheme used for [1]H NMR.

turn of the strands for an intermetallic distance of 8.8 Å (Fig. 4a). The 0.09 Å contraction of the Ln–N distances observed in going from nine-coordinated Eu^{III} (average Eu–N = 2.59(3) Å) to nine-coordinated Lu^{III} (average Lu–N = 2.50(2) Å) exactly fits the expected contraction of the ionic radii,[23] which logically results in identical bond valences $\nu_{Eu,N} = \nu_{Lu,N} = 0.32(2)$ within experimental errors (Tables S6–S8†).[24,25]

A thorough analysis of the successive helical pitches characterizing the overall helication of the ligand strands in $[Eu_2(\mathbf{L1})_3]^{6+}$ and $[Lu_2(\mathbf{L10})_3]^{6+}$ indicates that the rigidification of the ligand in **L10** has negligible structural consequences (Appendix 1). However, the use of larger La^{III} cations results in the fixation of two additional axial triflate anions to give $[La_2(\mathbf{L10})_3(CF_3SO_3)_2]^{4+}$ where (i) each metal is ten-coordinated, (ii) the bonding affinities of the heterocyclic nitrogen atoms are reduced (average bond valence $\nu_{La,N} = 0.27(2)$, Tables S6 and S7†), (iii) the helical pitches are reduced by more than 1 Å within the terminal sections without affecting the intermetallic distance (Appendix 1) and (iv) the area of the triangle defined by the three terminal nitrogen atoms increases from 4.71 Å^2 in $[Lu_2(\mathbf{L10})_3]^{6+}$ to 8.19 Å^2 in $[La_2(\mathbf{L10})_3(CF_3SO_3)_2]^{4+}$ (Fig. 4b). In the absence of related molecular structures reported for La(III) interacting with **L1**, the considerable changes induced by the coordination of large lanthanum cations in the triple-stranded architecture cannot be unambiguously assigned to the presence of rigid terminal phenanthroline units in **L10**.

Speciation and thermodynamics for helicate self-assemblies in solution

ESI-MS titrations of **L10** with $Ln(CF_3SO_3)_3 \cdot xH_2O$ in acetonitrile show the formation of $[Ln_2(\mathbf{L10})_3]^{6+}$, $[Ln_2(\mathbf{L10})_2]^{6+}$ and $[Ln_2(\mathbf{L10})]^{6+}$ for Ln = La, Eu in the gas-phase, together with an additional complex $[Ln_3(\mathbf{L10})_2]^{9+}$ for Ln = Lu (Tables S9–S11†). In solution, [1]H NMR titrations confirm the formation of intricate mixtures of complexes in the intermediate exchange rate on the NMR time scale with the emergence of the threefold-symmetrical $[Ln_2(\mathbf{L10})_3]^{6+}$ complexes as the only species for $|Ln|_{tot}/|\mathbf{L10}|_{tot} = 0.67$ at millimolar concentrations (10 aromatic signals, Fig. 2b). The unusual downfield shift monitored

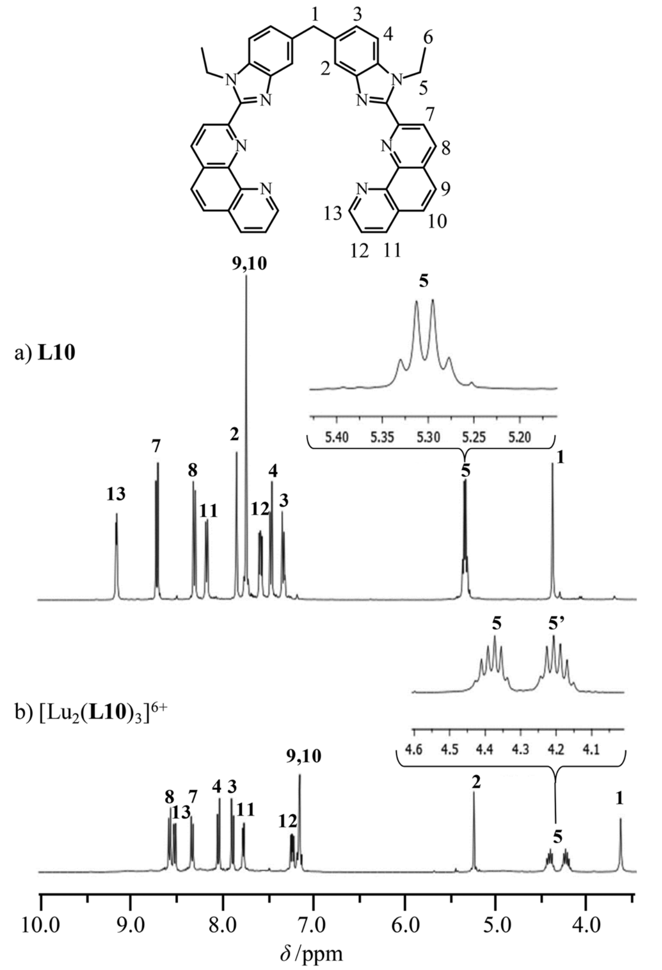

Fig. 2 Part of the ^{1}H NMR spectra recorded for (a) **L10** in $CDCl_3$ and (b) $[Lu_2(\mathbf{L10})_3]^{6+}$ in CD_3CN at 298 K ($|\mathbf{L10}|_{tot}$ = 0.5 mM). The transformation of the enantiotopic methylene protons H5,5′ (quartet) into their diastereotopic form (two pseudo-sextets) is highlighted.

for the signal of the aromatic proton H2 in the diamagnetic complexes ($\Delta\delta = \delta_{complex} - \delta_{ligand} = -1.90$ ppm for Ln = La and −2.57 for Ln = Lu) is diagnostic of the helication of the strands, which puts this proton into the shielding domain of the benzimidazole ring of an adjacent strand (Fig. 2).[26] The observation of diastereotopic H5,5′ methylene protons further confirms the non-planar arrangement of the strands, while the enantiotopic H1,1′ protons indicate the existence of three twofold axes perpendicular to the threefold axis (Fig. 2b), in line with the standard D_3-symmetry point group adopted by the relaxed triple-helical $[Ln_2(\mathbf{L10})_3]^{6+}$ complexes in solution. Interestingly, complexation of **L10** with Ln^{3+} is accompanied by *trans* to *cis* conformational changes about the phenanthroline–benzimidazole interaromatic bonds, which alters the envelope of the electronic absorption spectrum produced by ligand-centred n→π* and π→π* transitions (Fig. 5).

Factor analysis[27] applied to the spectrophotometric titrations of **L10** with $Ln(CF_3SO_3)_3{\cdot}xH_2O$ suggests the formation of three absorbing complexes $[Ln_2(\mathbf{L10})_3]^{6+}$, $[Ln_2(\mathbf{L10})_2]^{6+}$ and $[Ln_2(\mathbf{L10})]^{6+}$ for Ln = La, Eu together with an additional

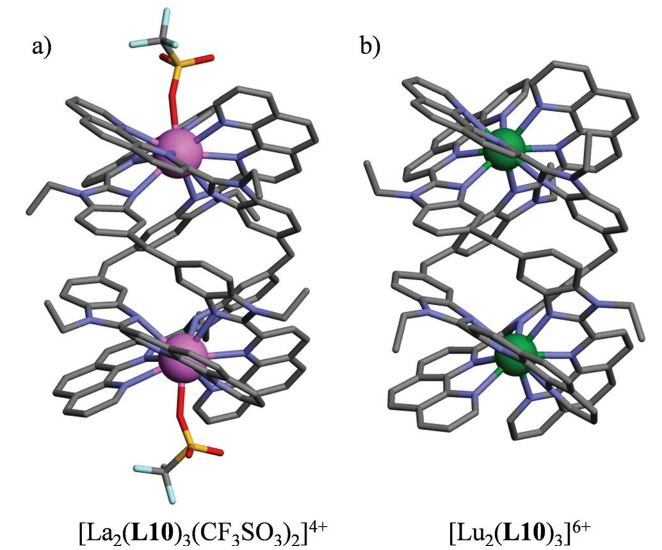

Fig. 3 Perspective views of the molecular structures of (a) $[La_2(\mathbf{L10})_3(CF_3SO_3)_2]^{4+}$ and (b) $[Lu_2(\mathbf{L10})_3]^{6+}$ observed in the crystal structures of $[La_2(\mathbf{L10})_3(CF_3SO_3)_2](CF_3SO_3)_4(CH_3CN)_6(C_6H_6)_6$ (**5**) and $[Lu_2(\mathbf{L10})_3](CF_3SO_3)_6(CH_3CN)_4$ (**6**). Color code: grey = C, blue = N, red = O, yellow = S, light blue = F, green = Lu, pink = La. Hydrogen atoms are omitted for clarity.

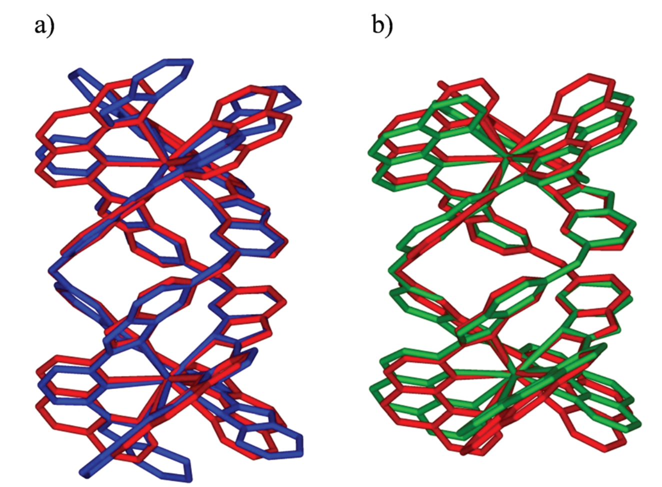

Fig. 4 Superimposition of (a) $[Lu_2(\mathbf{L10})_3]^{6+}$ (red) and $[Eu_2(\mathbf{L1})_3]^{6+}$ (blue) and (b) $[Lu_2(\mathbf{L10})_3]^{6+}$ (red) and $[La_2(\mathbf{L10})_3(CF_3SO_3)_2]^{4+}$ (green). Peripheral substituents connected to the ligand strands and terminal triflate anions are omitted for clarity.

$[Ln_3(\mathbf{L10})_2]^{9+}$ complex for Ln = Lu^{3+}, in complete agreement with the speciation detected by ESI-MS in the gas-phase. The global spectrophotometric data can be fitted with non-linear least-squares techniques to three macroscopic equilibria for Ln = La, Eu (eqn (2)–(4)) and to four macroscopic equilibria for Ln = Lu (eqn (2)–(5); Table 1).[28]

$$2Ln^{3+} + 3\mathbf{L10} \rightleftharpoons [Ln_2(\mathbf{L10})_3]^{6+} \quad \beta_{2,3}^{Ln,\mathbf{L10}} \tag{2}$$

$$2Ln^{3+} + 2\mathbf{L10} \rightleftharpoons [Ln_2(\mathbf{L10})_2]^{6+} \quad \beta_{2,2}^{Ln,\mathbf{L10}} \tag{3}$$

$$2Ln^{3+} + \mathbf{L10} \rightleftharpoons [Ln_2(\mathbf{L10})]^{6+} \quad \beta_{2,1}^{Ln,\mathbf{L10}} \tag{4}$$

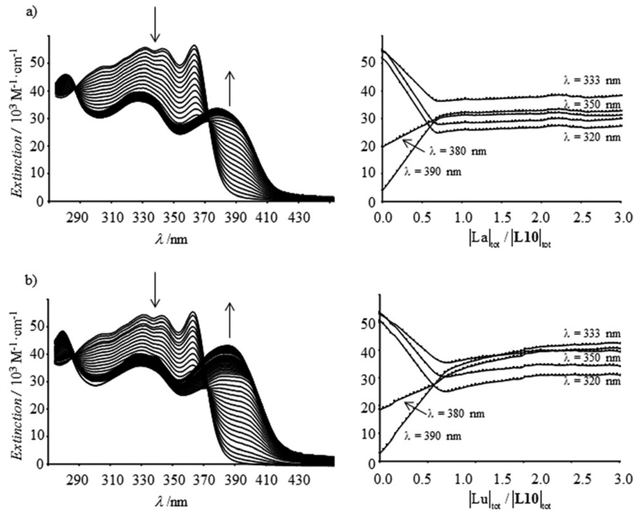

Fig. 5 Variation of absorption spectra (left) and corresponding variation of observed molar extinctions at 5 different wavelengths (right) observed for the spectrophotometric titrations of **L10** with (a) $La(CF_3SO_3)_3 \cdot 2H_2O$ and (b) $Lu(CF_3SO_3)_3 \cdot H_2O$ (total ligand concentration: 5×10^{-4} M in acetonitrile–chloroform (9 : 1); 298 K).

Table 1 Cumulative thermodynamic formation constants $\log(\beta_{2,n}^{\mathrm{Ln},\mathbf{L}k})$ obtained for $[\mathrm{Ln}_2(\mathbf{L}k)_n]^{6+}$ (**L*k*** = **L1**, **L2**, **L10**; Ln = La, Eu, Lu; 298 K)

Metal	Solvent	La	Eu	Lu	Reference
$\log(\beta_{2,3}^{\mathrm{Ln},\mathbf{L1}})$	CH_3CN	20–22	24.3(4)	^{a}	29
$\log(\beta_{2,2}^{\mathrm{Ln},\mathbf{L1}})$	CH_3CN	—	18.1(3)	^{a}	29
$\log(\beta_{2,3}^{\mathrm{Ln},\mathbf{L2}})$	CH_3CN	25.1(2)	26.0(2)	25.4(5)	30
$\log(\beta_{2,2}^{\mathrm{Ln},\mathbf{L2}})$	CH_3CN	19.2(5)	19.6(2)	19.3(4)	30
$\log(\beta_{2,3}^{\mathrm{Ln},\mathbf{L10}})$	$CH_3CN–CHCl_3$ (9 : 1)^b	24.8(5)	24.8(5)	24.7(2)	This work
$\log(\beta_{2,2}^{\mathrm{Ln},\mathbf{L10}})$	$CH_3CN–CHCl_3$ (9 : 1)^b	16.9(9)	16.9(9)	17.2(6)	This work
$\log(\beta_{3,2}^{\mathrm{Ln},\mathbf{L10}})$	$CH_3CN–CHCl_3$ (9 : 1)^b	—	—	23.4(2)	This work
$\log(\beta_{2,1}^{\mathrm{Ln},\mathbf{L10}})$	$CH_3CN–CHCl_3$ (9 : 1)^b	10.9(8)	10.9(8)	12.2(2)	This work

^{a} A partial fit of the spectrophotometric titration of **L1** with $Lu(ClO_4)_3$ suggested $\log(\beta_{2,3}^{\mathrm{Lu},\mathbf{L1}})$ = 17.5(4) in the absence of a satisfying model of Lu/**L1** > 0.67.[29] ^{b} +0.01 m $^n\mathrm{Bu_4NClO_4}$.

$$3\mathrm{Ln}^{3+} + 2\mathbf{L10} \rightleftharpoons [\mathrm{Ln}_3(\mathbf{L10})_2]^{9+} \quad \beta_{3,2}^{\mathrm{Ln},\mathbf{L10}} \tag{5}$$

The stability constants $\log(\beta_{2,3}^{\mathrm{Ln},\mathbf{L10}}) \approx 24.8$ found for the triple-helical complexes $[\mathrm{Ln}_2(\mathbf{L10})_3]^{6+}$ compare well with related values previously collected for $[\mathrm{Ln}_2(\mathbf{L1})_3]^{6+}$ and $[\mathrm{Ln}_2(\mathbf{L2})_3]^{6+}$ under similar conditions (Table 1).[29,30] Within the frame of the site-binding approach, the cumulative formation macroconstant given in eqn (2) can be modeled with eqn (6).[16,31]

$$\beta_{2,3}^{\mathrm{Ln},\mathbf{L10}} = \omega_{2,3}^{\mathrm{Ln},\mathbf{L10}} \left(f_{\mathrm{N_3}}^{\mathrm{Ln},\mathbf{L10}}\right)^6 \left(\mathrm{EM}^{\mathrm{Ln},\mathbf{L10}}\right)^2 \left(u_{\mathrm{Ln}}^{\mathbf{L10},\mathbf{L10}}\right)^6 u_{\mathbf{L10}}^{\mathrm{Ln},\mathrm{Ln}} \tag{6}$$

In this equation, $\omega_{2,3}^{\mathrm{Ln},\mathbf{L10}} = 96$ is the statistical factor of the assembly process, which takes into account the pure entropic contribution due to a change in molecular rotational entropies occurring upon complexation (Fig. S2†),[32] and $f_{\mathrm{N_3}}^{\mathrm{Ln},\mathbf{L10}}$ corresponds to the absolute intermolecular affinities of the tridentate heterocyclic N_3 binding unit for the entering Ln^{3+} cation. Each tridentate unit is considered to be bound to the lanthanide cation *via* a single point connector, and the associated free energy change $\Delta G_{\mathrm{N_3}}^{\mathrm{Ln},\mathbf{L10}} = -RT\ln\left(f_{\mathrm{N_3}}^{\mathrm{Ln},\mathbf{L10}}\right)$ includes the necessary solvent reorganization. Among the six Ln–N_3 binding events occurring in $[\mathrm{Ln}_2(\mathbf{L10})_3]^{6+}$, four are intermolecular and characterized with $f_{\mathrm{N_3}}^{\mathrm{Ln},\mathbf{L10}}$, but two are intramolecular (= macrocyclization) and their affinities must be corrected by using the effective molarity $f_{\mathrm{N_3,intra}}^{\mathrm{Ln},\mathbf{L10}} = f_{\mathrm{N_3}}^{\mathrm{Ln},\mathbf{L10}} \cdot \mathrm{EM}^{\mathrm{Ln},\mathbf{L10}}$. Finally, $u_{\mathrm{Ln}}^{\mathbf{L10},\mathbf{L10}} = e^{-\left(\Delta E_{\mathrm{Ln}}^{\mathbf{L10},\mathbf{L10}}/RT\right)}$ and $u_{\mathbf{L10}}^{\mathrm{Ln},\mathrm{Ln}} = e^{-\left(\Delta E_{\mathbf{L10}}^{\mathrm{Ln},\mathrm{Ln}}/RT\right)}$ are the Boltzmann factors correcting the free energy of connection for intramolecular ligand–ligand (*i.e.* **L10**···**L10**), respectively metal–metal (*i.e.* Ln···Ln) interactions resulting from the close location of two ligands, respectively two cations in $[\mathrm{Ln}_2(\mathbf{L10})_3]^{6+}$.[16,31] Obviously, the same model applies for $[\mathrm{Ln}_2(\mathbf{L1})_3]^{6+}$ (eqn (7)) and the extreme similarity of the crystal structures of the triple-helical cores in $[\mathrm{Eu}_2(\mathbf{L1})_3]^{6+}$ and $[\mathrm{Ln}_2(\mathbf{L10})_3]^{6+}$ lead us assume that (i) the intermolecular affinity of the tridentate binding units ($f_{\mathrm{N_3}}^{\mathrm{Ln},\mathbf{L1}} \approx f_{\mathrm{N_3}}^{\mathrm{Ln},\mathbf{L10}}$), (ii) the interligand interactions ($u_{\mathrm{Ln}}^{\mathbf{L1},\mathbf{L1}} \approx u_{\mathrm{Ln}}^{\mathbf{L10},\mathbf{L10}}$) and (iii) the intermetallic interactions ($u_{\mathbf{L1}}^{\mathrm{Ln},\mathrm{Ln}} \approx u_{\mathbf{L10}}^{\mathrm{Ln},\mathrm{Ln}}$) are identical for **L1** and **L10**. The simple ratio of the incriminated stability constants thus reduces to the square of the ratio of their effective molarities (eqn (8)).

$$\beta_{2,3}^{\mathrm{Ln},\mathbf{L1}} = \omega_{2,3}^{\mathrm{Ln},\mathbf{L1}} \left(f_{\mathrm{N_3}}^{\mathrm{Ln},\mathbf{L1}}\right)^6 \left(\mathrm{EM}^{\mathrm{Ln},\mathbf{L1}}\right)^2 \left(u_{\mathrm{Ln}}^{\mathbf{L1},\mathbf{L1}}\right)^6 u_{\mathbf{L1}}^{\mathrm{Ln},\mathrm{Ln}} \tag{7}$$

$$\frac{\beta_{2,3}^{\mathrm{Ln},\mathbf{L10}}}{\beta_{2,3}^{\mathrm{Ln},\mathbf{L1}}} = \frac{\omega_{2,3}^{\mathrm{Ln},\mathbf{L10}} \left(f_{\mathrm{N_3}}^{\mathrm{Ln},\mathbf{L10}}\right)^6 \left(\mathrm{EM}^{\mathrm{Ln},\mathbf{L10}}\right)^2 \left(u_{\mathrm{Ln}}^{\mathbf{L10},\mathbf{L10}}\right)^6 u_{\mathbf{L10}}^{\mathrm{Ln},\mathrm{Ln}}}{\omega_{2,3}^{\mathrm{Ln},\mathbf{L1}} \left(f_{\mathrm{N_3}}^{\mathrm{Ln},\mathbf{L1}}\right)^6 \left(\mathrm{EM}^{\mathrm{Ln},\mathbf{L1}}\right)^2 \left(u_{\mathrm{Ln}}^{\mathbf{L1},\mathbf{L1}}\right)^6 u_{\mathbf{L1}}^{\mathrm{Ln},\mathrm{Ln}}} \approx \left(\frac{\mathrm{EM}^{\mathrm{Ln},\mathbf{L10}}}{\mathrm{EM}^{\mathrm{Ln},\mathbf{L1}}}\right)^2 \tag{8}$$

Introducing the experimental values of the formation constants found for Ln = Eu (Table 1), together with $\mathrm{EM}^{\mathrm{Eu},\mathbf{L1}} = 10^{-4.1}$ M,[17] eventually provides $\mathrm{EM}^{\mathrm{Eu},\mathbf{L10}} = 10^{-3.9(4)}$ M.

Conclusion

The removal of two torsional degrees of freedom in going from **L1** to **L10** has a minor structural and thermodynamic influence on the formation of the target triple-stranded lanthanide helicates $[\mathrm{Ln}_2(\mathbf{L}k)_3]^{6+}$. The solid state structures display a similar helical wrapping of the strands leading to comparable intermetallic separation (≈ 0.9 nm), while closely related ^{1}H NMR characteristics point to identical relaxed D_3-symmetrical structures in solution. The isolation of the unsaturated dinuclear triple-stranded $[\mathrm{La}_2(\mathbf{L10})_3(\mathrm{CF_3SO_3})_2]^{4+}$ helicate with the largest lanthanide is the only innovative point reported here for this class of compounds. However, the similitude of the Eu-complexes with **L1** and **L10** allowed for a detailed thermodynamic analysis, which led us to conclude that the effective molarity (EM ≈ 10^{-4} M) is not significantly affected by the increased rigidity found in **L10**. This result contrasts with the decrease of EM by three to five orders of magnitude observed for $[\mathrm{Ln}_2(\mathbf{L9}\text{-}2\mathrm{H})_3]$ despite the topological (four degrees of torsional freedom) and structural similitudes between **L9** and **L10** (Scheme 1). We therefore deduce that the increased rigidity in **L9** is not the origin of its reluctance for macrocyclization in the dinuclear triple-stranded helicate. We should however stress here that **L9** indeed reacts as its dianion [**L9**-2H]$^{2-}$ in the self-assembly of [Ln_2(**L9**-2H)$_3$], a molecular form prone to strongly interacting with the hydroxylic co-solvent required for solubility reasons. We then suspect that a particular conformation of the deprotonated ligand in its half-complexed form prior to macrocyclization (see Fig. 1, middle) combined with some reluctance to produce neutral [Ln_2(**L9**-2H)$_3$] helicates in polar acetonitrile–methanol is responsible for the extremely small effective molarity reported for these complexes.[18] After relying on purely entropic (Gaussian exploration of space)[33] or enthalpic (freely joined chains)[34] contributions for rationally tuning the effective molarity in metal-induced helicate self-assemblies,[16] we highlight here a third tool based on solvation effects, in which both enthalpy and entropy aspects may contribute.

Experimental

Solvents and starting materials

These were purchased from Fluka AG or Aldrich and used without further purification unless otherwise stated. 3,3′-Dinitro-4,4′di(*N*-ethyl)amino-diphenylmethane was prepared according to a literature procedure.[20] Acetonitrile and dichloromethane were distilled over calcium hydride, and tetrahydrofuran was distilled over sodium. The triflate salts Ln(CF_3SO_3)$_3$·$x$$H_2O$ (Ln = La, Eu, Lu; x = 2–4) were prepared from the corresponding oxides (99.99%) and dried according to published procedures.[35] The Ln content of solid salts was determined by complexometric titrations with Titriplex III (Merck) in the presence of urotropine and xylene orange.[36]

Preparation of 1,10-phenanthroline-*N*-oxide (1). 1,10-Phenanthroline (4.7 g, 26 mmol), concentrated acetic acid (30 mL), water (2 mL) and 30% hydrogen peroxide (3.2 mL) were stirred at 70 °C for 3 h. A second crop of 30% hydrogen peroxide (3.2 mL) was added and stirring was maintained at 70 °C for three more hours. After cooling to RT, a last batch of 30% hydrogen peroxide (2 mL) was added and the resulting mixture was stirred for 12 h. Evaporation under vacuum reduced the volume to 10 mL, fresh water (35 mL) was added and the mixture was concentrated to 10 mL, cooled to 0 °C and neutralized with potassium carbonate (50 g). The resulting yellow-brown solid was isolated and extracted with hot chloroform under reflux for 12 h (soxhlet). The org. layer was dried over magnesium sulfate and charcoal, filtered and evaporated to dryness to give 1,10-phenanthroline-*N*-oxide (**1**, 3.75 g, 19.1 mmol, yield = 73.5%) as a pale yellow solid. ^{1}H NMR ($CDCl_3$) δ/ppm: 9.32 (dd, ^3J = 4.3 Hz, ^4J = 1.6 Hz, 1H), 8.76 (dd, ^3J = 6.3 Hz, ^4J = 1.0 Hz, 1H), 8.24 (dd, ^3J = 8.2 Hz, ^4J = 1.6 Hz, 1H), 7.81 (dd, ^3J = 8.8 Hz, 1H), 7.75 (d, ^3J = 8.8 Hz, 1H), 7.75 (d, ^3J = 8.0 Hz, 1H), 7.67 (dd, ^3J = 8.0 Hz, ^3J = 4.3 Hz, 1H), 7.46 (dd, ^3J = 8.0 Hz, ^3J = 6.3 Hz, 1H). ESI-MS (CH_2Cl_2): m/z 197.1 $[M + H]^+$.

Preparation of 2-cyano-1,10-phenanthroline (2). 1,10-Phenanthroline-*N*-oxide (**1**, 5.6 g, 28.5 mmol) and potassium cyanide (5.6 g) were stirred for 15 min in water (50 mL). Benzoyl chloride (5.6 g) was dropwise added under stirring for 1 h at RT. The resulting precipitate was filtered, washed with water and crystallized from hot ethanol to give 2-cyano-1,10-phenanthroline (**2**, 4.3 g, 20.9 mmol, yield: 73%) as a cream solid. ^{1}H NMR ($CDCl_3$) δ/ppm: 9.28 (dd, 1H, ^3J = 4.3 Hz, ^4J = 1.7 Hz), 8.40 (d, 1H, ^3J = 8.2 Hz), 8.31 (dd, 1H, ^3J = 8.1 Hz, ^4J = 1.7 Hz), 7.97 (d, 1H, ^3J = 8.2 Hz), 7.96 (d, 1H, ^3J = 8.8 Hz), 7.85 (d, 1H, ^3J = 8.8 Hz), 7.74 (dd, 1H, ^3J = 8.1 Hz, ^3J = 4.3 Hz).

Preparation of 1,10-phenanthroline-2-carboxylic acid (3). 2-Cyano-1,10-phenanthroline (**2**, 1.0 g, 4.9 mmol) and sodium hydroxide (0.85 g, 21 mmol) were refluxed in ethanol–water (10 mL : 10 mL) until emission of a basic gas (starch paper). The cooled solution was acidified to pH = 3.8 with concentrated hydrochloric acid, ethanol evaporated and the resulting cream precipitate was filtered, washed with water and dried under vacuum to give 1,10-phenanthroline-2-carboxylic acid (**3**, 0.84 g, 3.7 mmol, yield = 77%). ^{1}H NMR (d^6-DMSO) δ/ppm: δ 9.15 (dd, 1H, ^3J = 1.6 Hz, ^3J = 4.3 Hz), 8.66 (d, 1H, ^3J = 8.3 Hz), 8.54 (dd, 1H, ^3J = 8.1 Hz, ^4J = 1.6 Hz), 8.35 (d, 1H, ^3J = 8.3 Hz), 8.09 (q, 2H, ^3J = 8.8 Hz), 7.83 (dd, 1H, ^3J = 8.1 Hz, ^3J = 4.3 Hz); ESI-MS (CH_3CN–H_2O–NEt_3): m/z 223.1 $[M - H]^-$.

Preparation of *N*,*N*′-(methylenebis(2-nitro-4,1-phenylene))bis(*N*-ethyl-1,10-phenanthroline-2-carboxamide) (4). 1,10-Phenanthroline-2-carboxylic acid (**3**, 4. 0 g, 18 mmol) was refluxed in thionyl chloride (160 mL) for 30 minutes and evaporated to dryness. 3,3′-Dinitro-4,4′-di(*N*-ethylamino)diphenylmethane (1.0 g, 3.0 mmol) and dry potassium carbonate (60 g) in dichloromethane–tetrahydrofuran (200 mL : 60 mL) were slowly added, and the resulting mixture was refluxed for 72 h. Water (150 mL) was slowly added to the cooled solution and the org. layer was separated, washed with half sat. aq. NH_4Cl (150 mL), water (150 mL) and brine (150 mL), dried with sodium sulfate and evaporated to dryness. The crude product was purified by column chromatography (silica; MeOH–CH_2Cl_2 2 : 98) to give *N*,*N*′-(methylenebis(2-nitro-4,1-phenylene))bis(*N*-ethyl-1,10-phenanthroline-2-carboxamide) (**4**, 1.7 g, 2.3 mmol, yield = 77%). ESI-MS (CH_3CN–MeOH): m/z 756.8 $[M + H]^+$.

Preparation of bis(1-ethyl-2-(1,10-phenanthrolin-2-yl)-1*H*-benzo[*d*]imidazol-5-yl)methane (L10). *N*,*N*′-(Methylenebis(2-nitro-4,1-phenylene))bis(*N*-ethyl-1,10-phenanthroline-2-carboxamide) (**4**, 0.41 g, 0.54 mmol), activated powdered iron (0.91 g, 16 mmol) and concentrated hydrochloric acid (25 mL) were dissolved in ethanol–water (70 mL : 25 mL) and refluxed for 48 h. Excess iron was separated and ethanol was evaporated under vacuum. Dichloromethane (300 mL) and Na_2H_2EDTA (11.1 g, 30.0 mmol) in water (200 mL) were added under stirring. Conc. aq. ammonia (24.5%) was dropwise added until pH = 7, followed by conc. H_2O_2 (30%, 3 mL). The pH was finally raised to 8.5. The org. layer was separated and the aq. phase was extracted with dichloromethane (3 × 100 mL). The combined org. phase was washed with water (300 mL), brine (300 mL), dried over Na_2SO_4 and evaporated to dryness. The crude product was purified by column chromatography (silica; MeOH–CH_2Cl_2 2 : 98→3 : 97) to give bis(1-ethyl-2-(1,10-phenanthrolin-2-yl)-1*H*-benzo[*d*]imidazol-5-yl)methane (**L10**, 0.15 g, 0.23 mmol, yield = 42%) as a white solid. ^{1}H NMR ($CDCl_3$) δ/ppm 9.73 (d, ^3J = 4.4 Hz, 2H), 8.69 (d, ^3J = 8.4 Hz, 2H), 8.28 (d, ^3J = 8.5 Hz, 2H), 8.15 (d, ^3J = 8.1 Hz, 2H), 7.82 (s, 2H), 7.71 (s, 4H), 7.55 (dd, ^3J = 8.5 Hz, ^3J = 4.4 Hz, 2H), 7.44 (d, ^3J = 8.3 Hz, 2H), 7.31 (d, ^3J = 8.4 Hz, 2H), 5.30 (q, ^3J = 7.0 Hz, 4H), 4.34 (s, 2H), 1.56 (t, ^3J = 7.0 Hz, 6H). ^{13}C NMR ($CDCl_3$) δ/ppm 150.4, 150.2, 149.9, 146.4, 145.4, 143.3, 136.5, 136.4, 135.8, 135.2, 128.9, 128.1, 127.1, 126.2, 125.1, 123.5, 123.0, 120.1, 110.2, 42.4, 41.1 ESI-MS (CH_2Cl_2): m/z 661.3 $[M + H]^+$, 1321.7 $[2M + H]^+$. Anal. Cald for $C_{43}H_{32}N_8{\cdot}CH_3OH$: C, 76.50; H, 4.96; N, 16.22. Found C, 76.62; H, 4.92; N, 16.09.

Preparation of the complexes $[Ln_2(\mathbf{L10})_3](CF_3SO_3)_6{\cdot}xH_2O{\cdot}yCHCl_3$ (Ln = La, x = 3, y = 3; Ln = Eu, x = 7, y = 0; Ln = Lu, x = 5, y = 0). A solution of **L10** (50 mg, 76 µmol) in chloroform (3 mL) was added to $Ln(CF_3SO_3)_3{\cdot}xH_2O$ (Ln = La, Eu, Lu; 0.67 equivalent) in acetonitrile (3 mL). After stirring for 12 h, the mixture was evaporated to dryness, dissolved in fresh acetonitrile and diethyl ether was slowly diffused to give microcrystals, which were filtered and dried under vacuum.

$[La_2(\mathbf{L10})_3](CF_3SO_3)_6(H_2O)_3(CHCl_3)_3$. Yield = 93%. ^{1}H NMR ($CDCN_3$–$CDCl_3$ 2 : 3) δ/ppm 8.70 (d, ^3J = 8 Hz, 2H), 8.52 (dd, ^3J = 8 Hz, ^4J = 4 Hz, 2H), 8.21 (d, ^3J = 4 Hz, 2H), 8.19 (d, ^3J = 8 Hz, 2H), 8.00 (d, ^3J = 8 Hz, 2H), 7.90 (d, ^3J = 8 Hz, 2H), 7.30 (q, ^3J = 8 Hz, ^3J = 4 Hz, 2H), 7.15 (s, 2H), 7.05 (^3J = 8 Hz, 2H), 5.91 (s, 2H), 4.04 (m, 4H), 4.18 (m, 2H), 3.60 (s, 2H), 0.78 (t, ^3J = 8 Hz, 6H). Anal. Cald for $La_2(C_{43}H_{32}N_8)_3(CF_3SO_3)_6(H_2O)_3(CHCl_3)_3$ (MM = 3566.7): C, 46.47; H, 2.97; N, 9.42. Found C, 46.78; H, 3.02; N, 9.40.

$[Eu_2(\mathbf{L10})_3](CF_3SO_3)_6(H_2O)_7$. Yield = 62%. ^{1}H NMR ($CDCN_3$–$CDCl_3$ 2 : 3) δ/ppm 14.75 (s, 2H), 7.82 (d, ^3J = 8 Hz, 2H), 7.45 (d, ^3J = 8 Hz, 2H), 6.58 (d, ^3J = 8 Hz, 2H), 5.88 (d, ^3J = 8 Hz, 2H), 5.65 (d, ^3J = 8 Hz, 2H), 5.58 (d, ^3J = 8 Hz, 2H), 4.99 (d, ^3J = 8 Hz, 2H), 4.36 (s, 2H), 3.50 (d, ^3J = 8 Hz, 2H), 2.65 (q, ^3J = 8 Hz, 4H), 1.40 (s, 2H; H1), −1.23 (t, ^3J = 8 Hz, 6H). Anal. Cald for $Eu_2(C_{43}H_{32}N_8)_3(CF_3SO_3)_6(H_2O)_7$ (MM = 3306.8): C, 49.03; H, 3.35; N, 10.17. Found C, 49.04; H, 3.18; N, 10.23.

$[Lu_2(\mathbf{L10})_3](CF_3SO_3)_6(H_2O)_5$. Yield = 93%. ^{1}H NMR ($CDCN_3$–$CDCl_3$ 2 : 3) δ/ppm 8.57 (d, ^3J = 8 Hz, 2H), 8.53 (dd, ^3J = 8 Hz, ^4J = 4 Hz, 2H), 8.26 (d, ^3J = 8 Hz, 2H), 8.06 (d, ^3J = 8 Hz, 2H), 7.89 (d, ^3J = 8 Hz, 2H), 7.80 (d, ^3J = 4 Hz, 2H), 7.22 (q, ^3J = 8 Hz, ^3J = 4 Hz, 2H), 7.13 (s, 2H), 5.25 (s, 2H), 4.32 (m, 2H), 4.18 (m, 2H), 3.60 (s, 2H), 0.67 (t, ^3J = 8 Hz, 6H). Anal. Cald for $Lu_2(C_{43}H_{32}N_8)_3(CF_3SO_3)_6(H_2O)_5$ (MM = 3316.8): C, 48.89; H, 3.22; N, 10.14. Found C, 48.91; H, 3.18; N, 10.40.

Slow diffusion of benzene into concentrated acetonitrile solutions of these complexes yielded pale yellow X-ray quality prisms for $[La_2(\mathbf{L10})_3(CF_3SO_3)_2](CF_3SO_3)_4(CH_3CN)_6(C_6H_6)_6$ (**5**) and $[Lu_2(\mathbf{L10})_3](CF_3SO_3)_6(CH_3CN)_4$ (**6**).

Spectroscopic and analytical measurements

Spectrophotometric titrations were performed with a J&M diode array spectrometer (Tidas series) connected to an external computer. In a typical experiment, 50 cm^3 of a 10^{-4} mol dm^{-3} solution of ligand in acetonitrile–chloroform (9 : 1) were titrated at 298 K with a 10^{-3} mol dm^{-3} solution of $Ln(CF_3SO_3)_3$ in acetonitrile–chloroform (9 : 1) in an inert atmosphere. After each addition of 0.20 mL, the absorbance was recorded using Hellma optrodes (optical path length 0.1 cm) immersed in the thermostated titration vessel and connected to the spectrometer. Mathematical treatment of the spectrophotometric titrations was performed with factor analysis and with the SPECFIT program.[28] ^{1}H and ^{13}C NMR spectra were recorded at 25 °C on Bruker Avance 400 MHz and Bruker DRX-500 MHz spectrometers. Chemical shifts were given in ppm with respect to TMS. Pneumatically-assisted electrospray (ESI-MS) mass spectra were recorded from 10^{-4} mol dm^{-3} solutions on Finnigan SSQ7000 and MDS Aciex API III instruments. Elemental analyses were performed by K.-L. Buchwalder from the Microchemical Laboratory of the University of Geneva.

X-ray crystallography

A summary of crystal data, intensity measurements and structure refinements for $[La_2(\mathbf{L10})_3(CF_3SO_3)_2](CF_3SO_3)_4(CH_3CN)_6(C_6H_6)_6$ (**5**) and $[Lu_2(\mathbf{L10})_3](CF_3SO_3)_6(CH_3CN)_4$ (**6**) is collected in Table S1 (ESI†). The crystals were mounted on quartz fibers with a protection oil. Cell dimensions and intensities were measured at 160 K on an Agilent Supernova diffractometer with mirror-monochromated Cu[Kα] radiation (λ = 1.54184 Å). Data were corrected for Lorentz and polarization effects and for absorption. The structures were solved by direct methods (SIR97),[37] and all other calculations were performed with ShelX97[38] systems and ORTEP3[39] programs. CCDC 933010 and CCDC 933011 contain the supplementary crystallographic data.

Acknowledgements

Financial support from the Swiss National Science Foundation is gratefully acknowledged.

Notes and references

1 (*a*) C.-A. Palma, M. Cecchini and P. Samori, *Chem. Soc. Rev.*, 2012, **41**, 3713; (*b*) J.-M. Lehn, *Angew. Chem., Int. Ed.*, 2013, **52**, 2836.

2 (*a*) J.-M. Lehn, *Supramolecular Chemistry*, VCH, Weinheim, New York, Basel, Cambridge, Tokyo, 1995; (*b*) E. C. Constable, in *Comprehensive Supramolecular Chemistry*, ed. J. L. Atwood, J. E. D. Davies, D. D. MacNicol and F. Vögtle, Pergamon, Oxford, 1996, ch. 6; (*c*) C. Piguet, G. Bernardinelli and G. Hopfgartner, *Chem. Rev.*, 1997, **97**, 2005; (*d*) M. Albrecht, *Chem. Rev.*, 2001, **101**, 3457; (*e*) M. J. Hannon and L. J. Childs, *Supramol. Chem.*, 2004, **16**, 7.

3 (*a*) C. Piguet, G. Bernardinelli and A. F. Williams, *Angew. Chem., Int. Ed. Engl.*, 1992, **31**, 1624. For comprehensive reviews, see: (*b*) M. Albrecht, M. Fiege and O. Osetska, *Coord. Chem. Rev.*, 2008, **252**, 812; (*c*) C. M. G. dos Santos, A. J. Harte, S. J. Quinn and T. Gunnlaugsson, *Coord. Chem. Rev.*, 2008, **252**, 2512; (*d*) C. Piguet and J.-C.

G. Bünzli, in *Handbook on the Physics and Chemistry of Rare Earths*, ed. K. A. Gschneidner Jr., J.-C. G. Bünzli and V. K. Pecharsky, Elsevier Science, Amsterdam, 2009, vol. 40, pp. 301–553; (*e*) C. Lincheneau, F. Stomeo, S. Comby and T. Gunnlaugsson, *Aust. J. Chem.*, 2011, **64**, 1315.

4 (*a*) N. Martin, J.-C. G. Bünzli, V. McKee, C. Piguet and G. Hopfgartner, *Inorg. Chem.*, 1998, **37**, 577; (*b*) C. Platas-Iglesias, M. Elhabiri, M. Hollenstein, J.-C. G. Bünzli and C. Piguet, *J. Chem. Soc., Dalton Trans.*, 2000, 2031; (*c*) R. Tripier, M. Hollenstein, M. Elhabiri, A.-S. Chauvin, G. Zucchi, C. Piguet and J.-C. G. Bünzli, *Helv. Chim. Acta*, 2002, **85**, 1915; (*d*) K. Zeckert, J. Hamacek, J.-P. Rivera, S. Floquet, A. Pinto, M. Borkovec and C. Piguet, *J. Am. Chem. Soc.*, 2004, **126**, 11589.

5 (*a*) M. Elhabiri, R. Scopelliti, J.-C. G. Buenzli and C. Piguet, *J. Am. Chem. Soc.*, 1999, **121**, 10747; (*b*) A.-S. Chauvin, S. Comby, B. Song, C. D. B. Vandevyver, F. Thomas and J.-C. G. Bünzli, *Chem.–Eur. J.*, 2007, **13**, 9515; (*c*) A.-S. Chauvin, S. Comby, B. Song, C. D. B. Vandevyver and J.-C. G. Bünzli, *Chem.–Eur. J.*, 2008, **14**, 1726; (*d*) E. Deiters, B. Song, A.-S. Chauvin, C. D. B. Vandevyver and J.-C. G. Bünzli, *New J. Chem.*, 2008, **32**, 1140.

6 A.-S. Chauvin, S. Comby, M. Baud, C. De Piano, C. Duhot and J.-C. G. Bünzli, *Inorg. Chem.*, 2009, **48**, 10687.

7 (*a*) T. B. Jensen, R. Scopelliti and J.-C. G. Bünzli, *Inorg. Chem.*, 2006, **45**, 7806; (*b*) T. B. Jensen, R. Scopelliti and J.-C. G. Bünzli, *Chem.–Eur. J.*, 2007, **13**, 8404; (*c*) T. B. Jensen, R. Scopelliti and J.-C. G. Bünzli, *Dalton Trans.*, 2008, 1027.

8 N. André, T. B. Jensen, R. Scopelliti, D. Imbert, M. Elhabiri, G. Hopfgartner, C. Piguet and J.-C. G. Bünzli, *Inorg. Chem.*, 2004, **43**, 515.

9 (*a*) J.-C. G. Bünzli, A.-S. Chauvin, C. D. B. Vandevyver, S. Bo and S. Comby, *Ann. N. Y. Acad. Sci.*, 2008, **1130**, 97; (*b*) B. Song, C. D. B. Vandevyver, A.-S. Chauvin and J.-C. G. Bünzli, *Org. Biomol. Chem.*, 2008, **6**, 4125; (*c*) J.-C. G. Bünzli, *Chem. Lett.*, 2009, 104.

10 J. L. Lessmann and W. deW. Horrocks Jr., *Inorg. Chem.*, 2000, **39**, 3114.

11 (*a*) S. Comby, F. Stomeo, C. P. McCoy and T. Gunnlaugsson, *Helv. Chim. Acta*, 2009, **92**, 2461; (*b*) F. Stomeo, C. Lincheneau, J. P. Leonard, J. E. O'Brien, R. D. Peacock, C. P. McCoy and T. Gunnlaugsson, *J. Am. Chem. Soc.*, 2009, **131**, 9636; (*c*) C. Lincheneau, R. D. Peacock and T. Gunnlaugsson, *Chem.–Asian J.*, 2010, **5**, 500.

12 T. K. Ronson, H. Adams, L. P. Harding, S. J. A. Pope, D. Sykes, S. Faulkner and M. D. Ward, *Dalton Trans.*, 2007, 1006.

13 (*a*) J. Hamacek, S. Blanc, M. Elhabiri, E. Leize, A. van Dorsselaer, C. Piguet and A. M. Albrecht-Gary, *J. Am. Chem. Soc.*, 2003, **125**, 1541; (*b*) M. Elhabiri, J. Hamacek, J.-C. G. Bünzli and A. M. Albrecht-Gary, *Eur. J. Inorg. Chem.*, 2004, 51; (*c*) M. Elhabiri, J. Hamacek, N. Humbert, J.-C. G. Bünzli and A. M. Albrecht-Gary, *New J. Chem.*, 2004, **28**, 1096.

14 (*a*) G. Ercolani, *J. Am. Chem. Soc.*, 2003, **125**, 16097; (*b*) G. Ercolani, *J. Phys. Chem. B*, 2003, **107**, 5052.

15 (*a*) G. Schwarzenbach, *Helv. Chim. Acta*, 1952, **35**, 2344; (*b*) A. W. Adamson, *J. Am. Chem. Soc.*, 1954, **76**, 1578; (*c*) A. E. Martell, *Adv. Chem. Ser.*, 1966, **62**, 272; (*d*) D. Munro, *Chem. Brt.*, 1977, **13**, 100; (*e*) E. L. Simmons, *J. Chem. Educ.*, 1979, **56**, 578; (*f*) C.-S. Chung, *J. Chem. Educ.*, 1984, **61**, 1062; (*g*) R. J. Motekaitis, A. E. Martell and R. A. Hancock, *Coord. Chem. Rev.*, 1994, **133**, 39.

16 C. Piguet, *Chem. Commun.*, 2010, **46**, 6209.

17 T. Riis-Johannessen, N. Dalla Favera, T. K. Todorova, S. M. Huber, L. Gagliardi and C. Piguet, *Chem.–Eur. J.*, 2009, **15**, 12702.

18 E. Terazzi, L. Guénée, B. Bocquet, J.-F. Lemonnier, N. Dalla Favera and C. Piguet, *Chem.–Eur. J.*, 2009, **15**, 12719.

19 E. J. Corey, A. L. Borror and T. Foglia, *J. Org. Chem.*, 1965, **30**, 288.

20 C. Piguet, G. Bernardinelli, B. Bocquet, A. Quattropanni and A. F. Williams, *J. Am. Chem. Soc.*, 1992, **114**, 7440.

21 C. Piguet, B. Bocquet and G. Hopfgartner, *Helv. Chim. Acta*, 1994, **77**, 931.

22 The ^{1}H NMR signals of protons H9 and H10 are accidentally isochronous.

23 R. D. Shannon, *Acta Crystallogr., Sect. A: Cryst. Phys., Diffr., Theor. Gen. Cryst.*, 1976, **32**, 751.

24 (*a*) I. D. Brown and D. Altermatt, *Acta Crystallogr., Sect. B: Struct. Sci.*, 1985, **41**, 244; (*b*) N. E. Breese and M. O'Keeffe, *Acta Crystallogr., Sect. B: Struct. Sci.*, 1991, **47**, 192; (*c*) I. D. Brown, *Acta Crystallogr., Sect. B: Struct. Sci.*, 1992, **48**, 553; (*d*) I. D. Brown, *The Chemical Bond in Inorganic Chemistry*, Oxford University Press, UK, 2002; (*e*) I. D. Brown, *Chem. Rev.*, 2009, **109**, 6858.

25 (*a*) A. Trzesowska, R. Kruszynski and T. J. Bartczak, *Acta Crystallogr., Sect. B: Struct. Sci.*, 2004, **60**, 174; (*b*) A. Trzesowska, R. Kruszynski and T. J. Bartczak, *Acta Crystallogr., Sect. B: Struct. Sci.*, 2005, **61**, 429; (*c*) F. Zocchi, *J. Mol. Struct. (THEOCHEM)*, 2007, **805**, 73.

26 (*a*) C. Piguet, E. Rivara-Minten, G. Hopfgartner and J.-C. G. Bünzli, *Helv. Chim. Acta*, 1995, **78**, 1541; (*b*) C. Piguet, J.-C. G. Bünzli, G. Bernardinelli, G. Hopfgartner, S. Petoud and O. Schaad, *J. Am. Chem. Soc.*, 1996, **118**, 6681.

27 E. R. Malinowski and D. G. Howery, *Factor Analysis in Chemistry*, Wiley, New York, Chichester, 1980.

28 (*a*) H. Gampp, M. Maeder, C. J. Meyer and A. D. Zuberbühler, *Talanta*, 1985, **23**, 1133; (*b*) H. Gampp, M. Maeder, C. J. Meyer and A. D. Zuberbühler, *Talanta*, 1986, **33**, 943.

29 C. Piguet, J.-C. G. Bünzli, G. Bernardinelli, G. Hopfgartner and A. F. Williams, *J. Am. Chem. Soc.*, 1993, **115**, 8197.

30 K. Zeckert, J. Hamacek, J.-P. Rivera, S. Floquet, A. Pinto, M. Borkovec and C. Piguet, *J. Am. Chem. Soc.*, 2004, **126**, 11589.

31 J. Hamacek, M. Borkovec and C. Piguet, *Dalton Trans.*, 2006, 1473.

32 (*a*) S. W. Benson, *J. Am. Chem. Soc.*, 1958, **80**, 5151; (*b*) W. F. Bailey and A. S. Monahan, *J. Chem. Educ.*, 1978,

55, 489; (*c*) G. Ercolani, C. Piguet, M. Borkovec and J. Hamacek, *J. Phys. Chem. B*, 2007, **111**, 12195.

33 J.-M. Senegas, S. Koeller and C. Piguet, *Chem. Commun.*, 2005, 2235.

34 G. Canard, S. Koeller, G. Bernardinelli and C. Piguet, *J. Am. Chem. Soc.*, 2008, **130**, 1025.

35 J. F. Desreux, in *Lanthanide Probes in Life, Chemical and Earth Sciences*, ed. J.-C. G. Bünzli and G. R. Choppin, Elsevier, Amsterdam, 1989, ch. 2, p. 43.

36 G. Schwarzenbach, *Complexometric Titrations*, Chapman & Hall, London, 1957, p. 8.

37 A. Altomare, M. C. Burla, M. Camalli, G. Cascarano, C. Giacovazzo, A. Guagliardi, G. Moliterni, G. Polidori and R. Spagna, *J. Appl. Crystallogr.*, 1999, **32**, 115.

38 G. M. Sheldrick, *SHELXL97 Program for the Solution and Refinement of Crystal Structures*, University of Göttingen, Germany, 1997.

39 ORTEP3 for Windows. L. J. Farrugia, *J. Appl. Crystallogr.*, 1997, **30**, 565.

Electronic Supplementary Material (ESI) for Dalton Transactions

Monitoring helical twists and effective molarities in dinuclear triple-stranded lanthanide helicates.

Patrick E. Ryan, Laure Guénée and Claude Piguet*

Supporting Information (15 pages)

Appendix 1: **Geometrical analysis of the helicity in $[La_2(L10)_3(CF_3SO_3)_2]^{4+}$ and $[Lu_2(L10)_3]^{6+}$.**

The triple-stranded molecular structures found in $[La_2(\mathbf{L10})_3(CF_3SO_3)_2]^{4+}$ and $[Lu_2(\mathbf{L10})_3]^{6+}$ are considered as made of six helical sections packed along a pseudo-threefold axis defined by the axis passing through the two metals (Figure A1-1). Each helical portion is defined by two almost parallel facial planes (average interplanar angles: 2.45(8)° for $[La_2(\mathbf{L10})_3(CF_3SO_3)_2]^{4+}$ and 1.5(1)° for $[Lu_2(\mathbf{L10})_3]^{6+}$), each plane containing a set of three nitrogen atoms related by the pseudo-threefold symmetry. The distance between the facial planes gives the linear progression $d(F_i\text{-}F_j)$ of the helix, while its rotation is measured by the average twist angle α_{ij} defined by the angular rotation between the projections of N*i* and N*j* belonging to the same ligand strand onto a plane perpendicular to the pseudo-threefold axis. The pitch P_{ij} is finally calculated as the ratio of axial over angular progressions along the helical axis $P_{ij} = d(F_i\text{-}F_j)/(\alpha_{ij}/360)$ (Tables A1-1-A1-2).[S1]

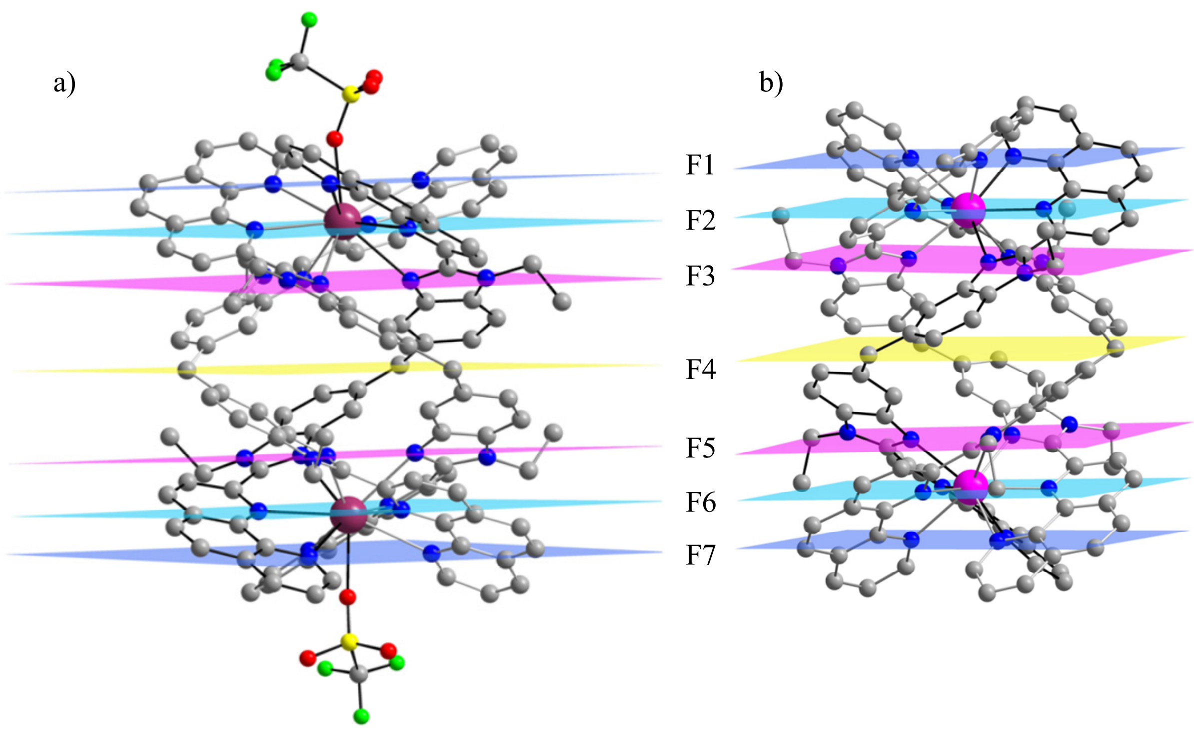

Figure A1-1 Representation of the facial planes in the molecular structures of (a) $[La_2(\mathbf{L10})_3(CF_3SO_3)_2]^{4+}$ and (b) $[Lu_2(\mathbf{L10})_3]^{6+}$.

Table A1-1 Helical pitches P_{ij}, linear distances $d(F_i\text{-}F_j)$ and average twist angle α_{ij} along the pseudo-C_3 axis[a] in the crystal structures of $[La_2(\mathbf{L10})_3(CF_3SO_3)_2](CF_3SO_3)_4(CH_3CN)_4(C_6H_6)$ (**5**) and $[Lu_2(\mathbf{L10})_3](CF_3SO_3)_6(CH_3CN)_3$ (**6**).

5 (La)	$d(F_i\text{-}F_j)$ /Å	α_{ij} /° [b]	P_{ij} /Å	**6** (Lu)	$d(F_i\text{-}F_j)$ /Å	α_{ij} /° [b]	P_{ij} /Å
F1-F2	1.36	53.7	9.12	F_1-F_2	1.606	56.6	10.21
F2-F3	1.65	53.2	11.17	F_2-F_3	1.622	54.9	10.64
F3-F4	2.64	61.9	15.35	F_3-F_4	2.846	61.06	16.78
F4-F5	2.64	61.9	15.35	F_4-F_5	2.846	61.06	16.78
F5-F6	1.65	52.2	11.37	F_5-F_6	1.622	54.90	10.64
F6-F7	1.36	54.7	8.95	F_6-F_7	1.606	56.62	10.21
F1-F7	11.30	338.4	12.02	F_1-F_7	12.148	345.14	12.67
Ln···Ln	8.9402(3)			8.8252(3)			

[a] Each helical portion F_1-F_2, F_2-F_3, F_3-F_4 and F_4-F_5 is characterised by (i) a linear extension $d(F_i\text{-}F_j)$ defined by the separation between the facial planes, (ii) an average twist angle α_{ij} defined by the angular rotation between the projections of N*i* and N*j* belonging to the same ligand strand and (iii) its pitch P_{ij} defined as $P_{ij} = d(F_i\text{-}F_j)/(\alpha_{ij}/360)$ (P_{ij} corresponds to the length of a cylinder containing a single turn of the helix defined by geometrical characteristics $d(F_i\text{-}F_j)$ and α_{ij}).[S1] [b] α_{ij} are given as C_3-average values.

Table A1-2 Helical pitches P_{ij}, linear distances $d(F_i\text{-}F_j)$ and average twist angle α_{ij} along the pseudo-C_3 axis[a] in the crystal structures of $[Eu_2(\mathbf{L1})_3](ClO_6)_6(CH_3CN)_6$.[3a]

Ln = Eu	$d(F_i\text{-}F_j)$ /Å	α_{ij} /° [b]	P_{ij} /Å
F1-F2	1.603	52.81	10.93
F2-F3	1.615	55.47	10.48
F3-F4	2.83	61.05	16.69
F4-F5	2.83	61.29	16.62
F5-F6	1.62	54.07	10.79
F6-F7	1.63	54.12	10.84
F1-F7	12.00	338.81	12.75
Ln···Ln	8.876(3)	-	-

[a] Each helical portion F_1-F_2, F_2-F_3, F_3-F_4 and F_4-F_5 is characterised by (i) a linear extension $d(F_i\text{-}F_j)$ defined by the separation between the facial planes, (ii) an average twist angle α_{ij} defined by the angular rotation between the projections of N*i* and N*j* belonging to the same ligand strand and (iii) its pitch P_{ij} defined as $P_{ij} = d(F_i\text{-}F_j)/(\alpha_{ij}/360)$ (P_{ij} corresponds to the length of a cylinder containing a single turn of the helix defined by geometrical characteristics $d(F_i\text{-}F_j)$ and α_{ij}).[S1] [b] α_{ij} are given as C_3-average values.

Reference

[S1] M. Cantuel, G. Bernardinelli, D. Imbert, J.-C. G. Bünzli, G. Hopfgartner and C. Piguet, *J. Chem. Soc.*, *Dalton Trans.*, **2002**, 1929 and references therein.

Table S1 Summary of crystal data, intensity measurements and structure refinements for $[La_2(\mathbf{L10})_3(CF_3SO_3)_2](CF_3SO_3)_4(CH_3CN)_6(C_6H_6)_6$ (**5**) and $[Lu_2(\mathbf{L10})_3](CF_3SO_3)_6(CH_3CN)_3$ (**6**).

	5	**6**
Empirical formula	$C_{183}H_{150}F_{18}La_2N_{30}O_{18}S_6$	$C_{143}H_{108}F_{18}Lu_2N_{28}O_{18}S_6$
Formula weight	3869.51	3390.86
Temperature	160(2) K	160(2) K
Wavelength	1.54184 Å	1.54184 Å
Crystal System, Space group	Monoclinic, *C*2/*c*	Monoclinic, *P*2/*c*
Unit cell dimensions	a = 32.4414(5) Å	a = 18.3243(3) Å
	b = 17.70112(17) Å	b = 23.0931(3) Å
	c = 33.7386(5) Å	c = 23.8096(4) Å
	α = 90°	α = 90°
	β = 117.1435(19)°	β = 130.3370(10)°
	γ = 90°	γ = 90°
Volume in $Å^3$	17240.6(4)	7680.0(2)
Z, Calculated density	4, 1.491 Mg/m^3	2, 1.466 Mg/m^3
Absorption coefficient	5.257 mm^{-1}	3.950 mm^{-1}
F(000)	7896	3412
Theta range for data collection	2.93 to 73.43°	3.10 to 73.62°
Limiting indices	$-40<=h<=39$,	$-17<=h<=22$,
	$-22<=k<=21$,	$-28<=k<=27$,
	$-41<=l<=34$	$-29<=l<=27$
Reflections collected / unique	50385 / 16936	33788 / 15190
	[R(int) = 0.0290]	[R(int) = 0.0294]
Completeness to theta	99.8 %	99.9 %
Data / restraints / parameters	16936 / 0 / 1054	15190 / 20 / 840
Goodness-of-fit on F^2	1.576	1.218
Final *R* indices [$I>2\sigma(I)$]	R_1 = 0.0502,	R_1 = 0.0595,
	ωR_2 = 0.1544	ωR_2 = 0.1831
R indices (all data)	R_1 = 0.0540,	R_1 = 0.0723,
	ωR_2 = 0.1598	ωR_2 = 0.1993
Largest diff. peak and hole	1.763 and -1.379 e.$Å^{-3}$	2.037 and -1.761 e.$Å^{-3}$

Table S2 Selected bond distances (Å), bond angles (°) in $[La_2(\mathbf{L10})_3(CF_3SO_3)_2](CF_3SO_3)_4(CH_3CN)_6(C_6H_6)_6$ (**5**).

Bond distances (Å)			
La(2A)-O(1)	2.520(3)	La(2A)-N(2B)	2.748(3)
La(2A)-N(3A)	2.694(3)	La(2A)-N(3B)	2.759(3)
La(2A)-N(2A)	2.719(3)	La(2A)-N(1A)	2.772(3)
La(2A)-N(7A)#1	2.734(3)	La(2A)-N(1B)	2.815(3)
La(2A)-N(5A)#1	2.743(3)	La(2A)···La(2A)#1	8.940(3)
La(2A)-N(8A)#1	2.744(3)		

Bond angles (°)			
O(1)-La(2A)-N(3A)	127.20(8)	N(2A)-La(2A)-N(3B)	134.38(8)
O(1)-La(2A)-N(2A)	92.37(8)	N(7A)#1-La(2A)-N(3B)	69.23(7)
N(3A)-La(2A)-N(2A)	60.86(8)	N(5A)#1-La(2A)-N(3B)	79.14(8)
O(1)-La(2A)-N(7A)#1	98.83(8)	N(8A)#1-La(2A)-N(3B)	69.21(8)
N(3A)-La(2A)-N(7A)#1	133.54(8)	N(2B)-La(2A)-N(3B)	60.81(8)
N(2A)-La(2A)-N(7A)#1	117.93(8)	O(1)-La(2A)-N(1A)	67.81(8)
O(1)-La(2A)-N(5A)#1	136.24(8)	N(3A)-La(2A)-N(1A)	119.11(8)
N(3A)-La(2A)-N(5A)#1	79.24(8)	N(2A)-La(2A)-N(1A)	59.86(8)
N(2A)-La(2A)-N(5A)#1	69.54(8)	N(7A)#1-La(2A)-N(1A)	68.87(8)
N(7A)#1-La(2A)-N(5A)#1	60.65(8)	N(5A)#1-La(2A)-N(1A)	68.68(8)
O(1)-La(2A)-N(8A)#1	65.58(9)	N(8A)#1-La(2A)-N(1A)	100.66(8)
N(3A)-La(2A)-N(8A)#1	140.22(8)	N(2B)-La(2A)-N(1A)	158.23(8)
N(2A)-La(2A)-N(8A)#1	155.87(8)	N(3B)-La(2A)-N(1A)	135.82(8)
N(7A)#1-La(2A)-N(8A)#1	59.89(8)	O(1)-La(2A)-N(1B)	61.40(8)
N(5A)#1-La(2A)-N(8A)#1	119.13(8)	N(3A)-La(2A)-N(1B)	67.10(8)
O(1)-La(2A)-N(2B)	90.48(9)	N(2A)-La(2A)-N(1B)	72.48(8)
N(3A)-La(2A)-N(2B)	72.17(8)	N(7A)#1-La(2A)-N(1B)	159.07(8)
N(2A)-La(2A)-N(2B)	122.26(8)	N(5A)#1-La(2A)-N(1B)	138.08(8)
N(7A)#1-La(2A)-N(2B)	118.48(8)	N(8A)#1-La(2A)-N(1B)	102.78(8)
N(5A)#1-La(2A)-N(2B)	133.09(9)	N(2B)-La(2A)-N(1B)	59.01(8)
N(8A)#1-La(2A)-N(2B)	70.13(8)	N(3B)-La(2A)-N(1B)	117.90(8)
O(1)-La(2A)-N(3B)	132.59(8)	N(1A)-La(2A)-N(1B)	106.25(8)
N(3A)-La(2A)-N(3B)	81.73(8)		

Symmetry transformation used to generate equivalent atoms: #1: $-x+1$, y, $-z+½$.

Table S3 Selected least-squares planes data for $[La_2(\mathbf{L10})_3(CF_3SO_3)_2](CF_3SO_3)_4(CH_3CN)_6(C_6H_6)_6$ (**5**).

Least-squares planes description	Abbreviation	Max. deviation/Å	Atom
Phenanthroline 1a	Phen1a		
N1 C1 C2 C3 C4 C5 C6 N2 C7 C8 C9 C10 N2 C11 C12		0.066(1)	N2a
Benzimidazole 1a	Bz1a		
N3 C13 N4 C16 C17 C18 C19 C20 C21		0.038(1)	N3a
Benzimidazole 2a	Bz2a		
C23 C24 C25 C26 N6 C27 N5 C28 C29		0.029(1)	N5a
Phenanthroline 2a	Phen2a		
C32 C33 C34 C35 C36 C37 C38 C39 C40 C41 N8 C42 C43 N7		0.082(1)	C40a
Phenanthroline 1b	Phen1b		
N1 C1 C2 C3 C4 C5 C6 N2 C7 C8 C9 C10 N2 C11 C12		0.062(1)	N1b
Benzimidazole 1b	Bz1b		
N3 C13 N4 C16 C17 C18 C19 C20 C21		0.045(1)	N3b

Interplanar angles (°)[a]

	Bz1a	Phen1b	Bz1b	Phen2a'	Bz2a'	Phen2a	Bz2a
Phen1a	40.2	55.5	57.0	49.6	19.0	34.5	58.2
Bz1a		25.3	54.5	61.8	54.7	61.5	55.2
Phen1b			37.0	50.8	62.8	60.5	37.2
Bz1b				18.3	50.6	36.8	1.2
Phen2a							37.7

The error is typically ±0.1°.

Electronic Supplementary Material (ESI) for Dalton Transactions

Table S4 Selected bond distances (Å), bond angles (°) in $[Lu_2(\mathbf{L10})_3](CF_3SO_3)_6(CH_3CN)_4$ (**6**).

Bond distances (Å)			
Lu(1)-N(3A)	2.475(3)	Lu(1)-N(5A)#1	2.513(4)
Lu(1)-N(2A)	2.486(4)	Lu(1)-N(8A)#1	2.522(5)
Lu(1)-N(2B)	2.489(4)	Lu(1)-N(1A)	2.524(4)
Lu(1)-N(7A)#1	2.499(4)	Lu(1)-N(1B)	2.535(4)
Lu(1)-N(3B)	2.499(4)	Lu(1) ···Lu(2)#1	8.8253(3)

Bond angles (°)			
N(3A)-Lu(1)-N(2A)	64.41(12)	N(7A)#1-Lu(1)-N(8A)#1	64.91(14)
N(3A)-Lu(1)-N(2B)	72.02(12)	N(3B)-Lu(1)-N(8A)#1	80.45(14)
N(2A)-Lu(1)-N(2B)	120.72(13)	N(5A)#1-Lu(1)-N(8A)#1	128.97(15)
N(3A)-Lu(1)-N(7A)#1	142.22(12)	N(3A)-Lu(1)-N(1A)	128.87(15)
N(2A)-Lu(1)-N(7A)#1	118.76(15)	N(2A)-Lu(1)-N(1A)	64.49(15)
N(2B)-Lu(1)-N(7A)#1	120.37(15)	N(2B)-Lu(1)-N(1A)	137.12(14)
N(3A)-Lu(1)-N(3B)	85.62(11)	N(7A)#1-Lu(1)-N(1A)	68.92(15)
N(2A)-Lu(1)-N(3B)	142.50(13)	N(3B)-Lu(1)-N(1A)	140.46(14)
N(2B)-Lu(1)-N(3B)	64.48(12)	N(5A)#1-Lu(1)-N(1A)	81.23(14)
N(7A)#1-Lu(1)-N(3B)	71.65(13)	N(8A)#1-Lu(1)-N(1A)	80.58(16)
N(3A)-Lu(1)-N(5A)#1	84.45(12)	N(3A)-Lu(1)-N(1B)	79.40(13)
N(2A)-Lu(1)-N(5A)#1	71.46(14)	N(2A)-Lu(1)-N(1B)	69.60(14)
N(2B)-Lu(1)-N(5A)#1	141.61(12)	N(2B)-Lu(1)-N(1B)	64.41(13)
N(7A)#1-Lu(1)-N(5A)#1	64.06(14)	N(7A)#1-Lu(1)-N(1B)	138.32(12)
N(3B)-Lu(1)-N(5A)#1	84.30(13)	N(3B)-Lu(1)-N(1B)	128.89(13)
N(3A)-Lu(1)-N(8A)#1	141.55(13)	N(5A)#1-Lu(1)-N(1B)	141.05(14)
N(2A)-Lu(1)-N(8A)#1	137.05(14)	N(8A)#1-Lu(1)-N(1B)	81.93(14)
N(2B)-Lu(1)-N(8A)#1	69.63(13)	N(1A)-Lu(1)-N(1B)	81.86(13)

Symmetry transformation used to generate equivalent atoms: #1: $-x+1$, y, $-z+3/2$.

Table S5 Selected least-squares planes data for $[Lu_2(\mathbf{L10})_3](CF_3SO_3)_6(CH_3CN)_4$ (**6**).

Least-squares planes description	Abbreviation	Max. deviation/Å	Atom
Phenanthroline 1a	Phen1a		
N1 C1 C2 C3 C4 C5 C6 N2 C7 C8 C9 C10 N2 C11 C12		0.130(1)	N2
Benzimidazole 1a	Bz1a		
N3 C13 N4 C16 C17 C18 C19 C20 C21		0.044(1)	N3
Benzimidazole 2a	Bz2a		
C23 C24 C25 C26 N6 C27 N5 C28 C29		0.034(1)	C29
Phenanthroline 2a	Phen2a		
C32 C33 C34 C35 C36 C37 C38 C39 C40 C41 N8 C42 C43 N7		0.146(1)	C40
Phenanthroline 1b	Phen1b		
N1 C1 C2 C3 C4 C5 C6 N2 C7 C8 C9 C10 N2 C11 C12		0.141(1)	C9
Benzimidazole 1b	Bz1b		
N3 C13 N4 C16 C17 C18 C19 C20 C21		0.045(1)	N3

Interplanar angles (°)[a]

	Bz1a	Phen1b	Bz1b	Phen2a'	Bz2a'	Phen2a	Bz2a
Phen1a	35.8	63.2	70.5	60.4	32.6	44.2	65.3
Bz1a		34.1	58.7	71.8	59.8	67.5	68.4
Phen1b			33.4	62.9	71.9	72.3	53.0
Bz1b				63.1	59.0	52.9	22.6
Phen2a							33.5

The error is typically ±0.1°.

Table S6 Bond Distances ($\delta_{i,j}$), bond Valences ($\nu_{\mathrm{Ln,j}}$)[a] and total atom valence (V_{Ln})[b] in the crystal structure of $[La_2(\mathbf{L10})_3(CF_3SO_3)_2](CF_3SO_3)_4(CH_3CN)_6(C_6H_6)_6$ (**5**).

Atom[c]	Donor type	$\delta_{\mathrm{La},j}$ / Å	$V_{\mathrm{La},j}$	
O(1)	Triflate	2.520	0.364	
N(3A)	Bzim	2.694	0.309	
N(2A)	Phen	2.719	0.289	
N(7A)#	Phen	2.734	0.278	
N(5A)#	Bzim	2.743	0.271	
N(8A)#	Phen	2.744	0.270	
N(2B)	Phen	2.748	0.267	
N(3B)	Bzim	2.759	0.260	
N(1A)	Phen	2.772	0.251	Average N-heterocyclic
N(1B)	Phen	2.815	0.223	0.27(2)
		V_{La}	2.783	

[a] $\nu_{\mathrm{Ln},j} = e^{\left[\left(R_{\mathrm{Ln},j} - d_{\mathrm{Ln},j}\right)/b\right]}$, whereby $\delta_{\mathrm{Ln},j}$ is the Ln-donor atom j distance. The valence bond parameters $R_{\mathrm{Ln,N}}$ and $R_{\mathrm{Ln,O}}$ are taken from ref 25 and b = 0.37 Å. [b] $V_{\mathrm{Ln}} = \sum_j \nu_{\mathrm{Ln},j}$. [c] Numbering taken from Fig S1a.

Table S7 Bond Distances ($\delta_{i,j}$), bond Valences ($\nu_{\mathrm{Ln,j}}$)[a] and total atom valence (V_{Ln})[b] in the crystal structure of $[Lu_2(\mathbf{L10})_3](CF_3SO_3)_6(CH_3CN)_4$ (**6**).

Atom[c]	Donor type	$\delta_{\mathrm{Lu},j}$ / Å	$V_{\mathrm{Lu},j}$	
N(3A)	Bzim	2.475	0.346	
N(2A)	Phen	2.486	0.336	
N(7A)#	Phen	2.489	0.333	
N(5A)#	Phen	2.499	0.324	
N(8A)#	Bzim	2.499	0.324	
N(2B)	Bzim	2.513	0.312	
N(3B)	Phen	2.522	0.304	
N(1A)	Phen	2.524	0.303	Average N-heterocyclic
N(1B)	Phen	2.535	0.294	0.32(2)
		V_{Lu}	2.875	

[a] $\nu_{\mathrm{Ln},j} = e^{\left[\left(R_{\mathrm{Ln},j} - d_{\mathrm{Ln},j}\right)/b\right]}$, whereby $\delta_{\mathrm{Ln},j}$ is the Ln-donor atom j distance. The valence bond parameter $R_{\mathrm{Ln,N}}$ is taken from ref 25 and b = 0.37 Å. [b] $V_{\mathrm{Ln}} = \sum_j \nu_{\mathrm{Ln},j}$. [c] Numbering taken from Fig S1b.

Table S8 Bond Distances ($\delta_{i,j}$), bond Valences ($v_{\mathrm{Ln,j}}$)[a] and total atom valence (V_{Ln})[b] in the crystal structure of $[Eu_2(\mathbf{L1})_3](ClO_4)_6(CH_3CN)_9$.[3a]

Atom[c]	Donor type	$\delta_{\mathrm{Eu1},j}$ / Å	$V_{\mathrm{Eu1},j}$	
N(1)A	Bzim	2.57	0.33	
N(3)A	Py	2.59	0.32	
N(4)A	Bzim	2.60	0.31	
N(1)B	Bzim	2.58	0.33	
N(3)B	Py	2.59	0.32	
N(4)B	Bzim	2.58	0.33	
N(1)C	Bzim	2.57	0.33	
N(3)C	Py	2.61	0.30	Average N-heterocyclic
N(4)C	Bzim	2.54	0.36	0.33(2)
		V_{Eu1}	2.927	
N(6)A	Bzim	2.57	0.33	
N(8)A	Py	2.58	0.33	
N(9)A	Bzim	2.67	0.26	
N(6)B	Bzim	2.61	0.30	
N(8)B	Py	2.64	0.28	
N(9)B	Bzim	2.60	0.31	
N(6)C	Bzim	2.61	0.30	
N(8)C	Py	2.58	0.33	Average N-heterocyclic
N(9)C	Bzim	2.59	0.32	0.31(3)
		V_{Eu2}	2.745	

[a] $v_{\mathrm{Ln},j} = e^{\left[\left(R_{\mathrm{Ln},j}-d_{\mathrm{Ln},j}\right)/b\right]}$, whereby $\delta_{\mathrm{Ln},j}$ is the Ln-donor atom j distance. The valence bond parameters $R_{\mathrm{Ln,N}}$ and $R_{\mathrm{Ln,O}}$ are taken from ref 25 and b = 0.37 Å. [b] $V_{\mathrm{Ln}} = \sum_j v_{\mathrm{Ln},j}$. [c] Numbering taken from ref. 3a.

Table S9 ESI-MS peaks observed for the titration of **L10** with $La(CF_3SO_3)_3$ in CH_3CN.

	m/z exp	*m/z* cald
$[La_2(\mathbf{L10})_3(Otf)_4]^{2+}$ [a]	1428.3	1428.2
$[La_2(\mathbf{L10})_2(Otf)_4]^{2+}$	1098.1	1097.9
$[La_2(\mathbf{L10})\ Otf)_4(CH_3OH)_4(CH_3CN)_4]^{2+}$	913.7	913.1
$[La_2(\mathbf{L10})_3(Otf)_3]^{3+}$	902.5	902.5
$[La_2(\mathbf{L10})(Otf)_4(CH_3OH)(CH_3CN)]^{2+}$	804.6	803.5
$[La_2(\mathbf{L10})_3(Otf)_2]^{4+}$	639.7	639.6
$[La_2(\mathbf{L10})(Otf)_3(CH_3OH)(CH_3CN)]^{3+}$	485.1	486.0
$[La_2(\mathbf{L10})_3(Otf)]^{5+}$	482.2	481.9
$[La_2(\mathbf{L10})\ (Otf)_2(CH_3OH)_5(CH_3CN)_4]^{4+}$	390.6	390.1
$[La_2(\mathbf{L10})_3(Otf)]^{6+}$	377.0	376.4
$[La_2(\mathbf{L10})(Otf)_2(CH_3OH)_3(CH_3CN)_4]^{4+}$	374.3	374.0

[a] $Otf^- = CF_3SO_3^-$

Table S10 ESI-MS peaks observed for the titration of **L10** with $Eu(CF_3SO_3)_3$ in CH_3CN.

	m/z exp	*m/z* cald
$[Eu_2(\mathbf{L10})_3(Otf)_4]^{2+}$ [a]	1441.4	1441.3
$[Eu_2(\mathbf{L10})_2(Otf)_4]^{2+}$	1111.0	1110.9
$[Eu_2(\mathbf{L10})_3(Otf)_3]^{3+}$	911.2	911.2
$[Eu_2(\mathbf{L10})_3(Otf)_2]^{4+}$	646.7	646.1
$[Eu_2(\mathbf{L10})(Otf)_3(CH_3OH)_3]^{3+}$	503.2	503.0
$[Eu_2(\mathbf{L10})_3(Otf)]^{5+}$	487.4	487.1
$[Eu_2(\mathbf{L10})(Otf)_2(CH_3OH)_5(CH_3CN)_{10}]^{4+}$	458.6	458.7
$[Eu_2(\mathbf{L10})(Otf)_2(CH_3OH)_7(CH_3CN)_3]^{4+}$	402.0	402.8
$[Eu_2(\mathbf{L10})_3]^{6+}$	381.2	381.1

[a] $Otf^- = CF_3SO_3^-$

Table S11 ESI-MS peaks observed for the titration of **L10** with $Lu(CF_3SO_3)_3$ in CH_3CN.

	m/z exp	*m/z* cald
$[Lu_2(\mathbf{L10})(Otf)_5(CH_3CN)]^{+}$ [a]	1795.9	1795.3
$[Lu_2(\mathbf{L10})_3(Otf)_4]^{2+}$	1464.2	1464.3
$[Lu_2(\mathbf{L10})_2(Otf)_4]^{2+}$	1133.6	1133.9
$[Lu_3(\mathbf{L10})_2(Otf)_6(CH_3OH)(CH_3CN)]^{3+}$	937.4	938.0
$[Lu_2(\mathbf{L10})_3(Otf)_3]^{3+}$	926.7	926.5
$[Lu_2(\mathbf{L10})(Otf)_4(CH_3CN)]^{2+}$	822.6	823.5
$[Lu_3(\mathbf{L10})_2(Otf)_5(CH_3OH)(CH_3CN)]^{4+}$	665.5	665.8
$[Lu_2(\mathbf{L10})_3(Otf)_2]^{4+}$	657.7	657.6
$[Lu_2(\mathbf{L10})(Otf)_3(CH_3CN)_2]^{3+}$	513.0	513.0
$[Lu_2(\mathbf{L10})(Otf)_3(CH_3OH)(CH_3CN)]^{3+}$	509.9	510.0
$[Lu_3(\mathbf{L10})_2(Otf)_4(CH_3OH)(CH_3CN)]^{5+}$	502.8	502.9
$[Lu_2(\mathbf{L10})(Otf)_3(CH_3CN)]^{3+}$	500.2	499.3
$[Lu_2(\mathbf{L10})_3(Otf)]^{5+}$	496.6	496.3
$[Lu_2(\mathbf{L10})(Otf)_2(CH_3OH)_6(CH_3CN)_4]^{4+}$	416.2	416.1
$[Lu_2(\mathbf{L10})(Otf)_2(CH_3OH)_4(CH_3CN)_5]^{4+}$	409.6	410.3
$[Lu_3(\mathbf{L10})_2(Otf)_3(CH_3CN)_6]^{6+}$	395.7	395.7
$[Lu_2(\mathbf{L10})_3]^{6+}$	389.0	388.7

[a] $Otf^- = CF_3SO_3^-$

Electronic Supplementary Material (ESI) for Dalton Transactions
This journal is © The Royal Society of Chemistry 2013

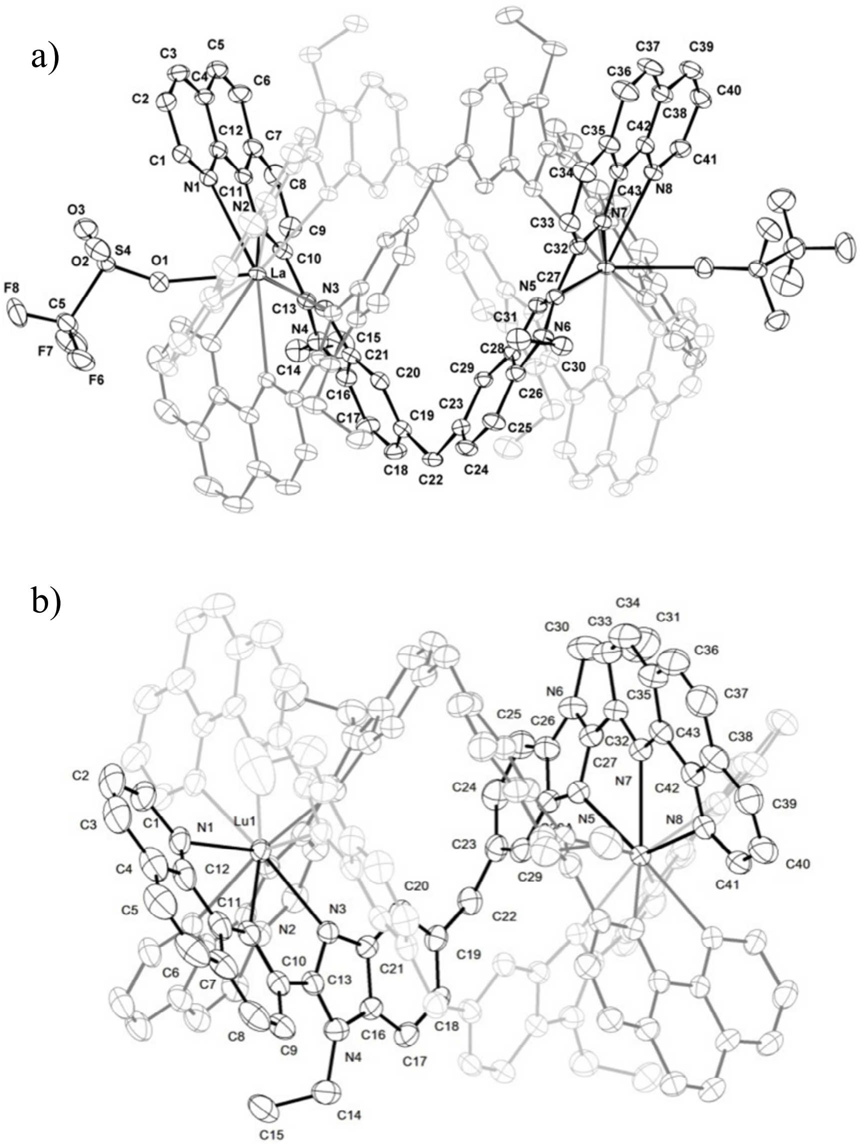

Figure S1 Molecular structures with partial numbering schemes of (a) $[La_2(\mathbf{L10})_3(CF_3SO_3)_2]^{4+}$ and (b) $[Lu_2(\mathbf{L10})_3]^{6+}$ observed in the crystal structures of $[La_2(\mathbf{L10})_3(CF_3SO_3)_2](CF_3SO_3)_4(CH_3CN)_6(C_6H_6)_6$ (**5**) and $[Lu_2(\mathbf{L10})_3](CF_3SO_3)_6(CH_3CN)_4$ (**6**) (thermal ellipsoids are represented at the 30% probability level). Hydrogen atoms are omitted for clarity.

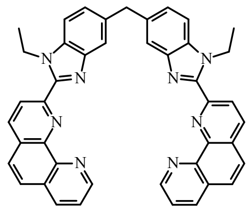

$$2\,[\mathrm{Ln(CH_3CN)_9}]^{2+} + 3\,\mathbf{L10} \underset{\beta_{1,2}^{\mathrm{Ln},\mathbf{L7}}}{\rightleftharpoons} [\mathrm{Ln_2}(\mathbf{L10})_3]^{3+} + 18\,\mathrm{CH_3CN}$$

Point groups:	D_{3h}	C_{2v}	D_3	C_{3v}
σ^{ext}:	6	2	6	3
σ^{int}:	3^9	3^2	3^6	1
σ^{chiral}:	1	1	1/2	1

$$\omega_{2,3}^{\mathrm{Ln},\mathbf{L10}} = \frac{\left(\sigma_{\mathrm{Ln}}^{\mathrm{ext}}\sigma_{\mathrm{Ln}}^{\mathrm{int}}\sigma_{\mathrm{Ln}}^{\mathrm{chiral}}\right)^2\cdot\left(\sigma_{\mathbf{L10}}^{\mathrm{ext}}\sigma_{\mathbf{L10}}^{\mathrm{int}}\sigma_{\mathbf{L10}}^{\mathrm{chiral}}\right)^3}{\left(\sigma_{\mathrm{complex}}^{\mathrm{ext}}\sigma_{\mathrm{complex}}^{\mathrm{int}}\sigma_{\mathrm{complex}}^{\mathrm{chiral}}\right)\cdot\left(\sigma_{\mathrm{CH_3CN}}^{\mathrm{ext}}\sigma_{\mathrm{CH_3CN}}^{\mathrm{int}}\sigma_{\mathrm{CH_3CN}}^{\mathrm{chiral}}\right)^{18}} = \frac{\left(6\cdot 3^9\right)^2\left(2\cdot 3^2\right)^3}{6\cdot \frac{1}{2}\cdot 3^6\cdot 3^{18}} = 96$$

$$\Rightarrow \beta_{2,3}^{\mathrm{Ln},\mathbf{L10}} = 96\left(f_{\mathrm{N_3}}^{\mathrm{Ln},\mathbf{L10}}\right)^6\left(EM^{\mathrm{Ln},\mathbf{L10}}\right)^2\left(u_{\mathrm{Ln}}^{\mathbf{L10},\mathbf{L10}}\right)^6 u_{\mathbf{L10}}^{\mathrm{Ln,Ln}} \quad (5)$$

Figure S2 Symmetry numbers (σ) and statistical factors (ω) for the complexation of $[\mathrm{Ln(CH_3CN)_9}]^{3+}$ with **L10** in acetonitrile.[32]